

Multimodal mapping of the face connectome

Yin Wang^{1,6*}, Athanasia Metoki^{2,6}, David V. Smith², John D. Medaglia^{3,4}, Yinyin Zang⁵, Susan Benear², Haroon Popal², Ying Lin² and Ingrid R. Olson^{2*}

Face processing supports our ability to recognize friend from foe, form tribes and understand the emotional implications of changes in facial musculature. This skill relies on a distributed network of brain regions, but how these regions interact is poorly understood. Here we integrate anatomical and functional connectivity measurements with behavioural assays to create a global model of the face connectome. We dissect key features, such as the network topology and fibre composition. We propose a neurocognitive model with three core streams; face processing along these streams occurs in a parallel and reciprocal manner. Although long-range fibre paths are important, the face network is dominated by short-range fibres. Finally, we provide evidence that the well-known right lateralization of face processing arises from imbalanced intra- and interhemispheric connections. In summary, the face network relies on dynamic communication across highly structured fibre tracts, enabling coherent face processing that underpins behaviour and cognition.

Face perception is a highly developed skill in humans owing to its unique evolutionary and social importance. From a brief glance at a face, we are able to effortlessly glean information about a person's age, gender, identity, social group, emotional state, attentional focus and several other characteristics such as trustworthiness¹.

Early studies on patients with focal brain lesions revealed that portions of the inferior temporal cortex in the right hemisphere might be critical for face processing, as damage to this region often resulted in the clinical syndrome of prosopagnosia¹. Lesion work gave way to single-unit recording and functional magnetic resonance imaging (fMRI) studies that documented a distributed set of specialized face patches^{2–4}. Many of these patches run along the ventral visual stream to the temporal pole, with more posterior regions processing fundamental aspects of faces (for example, the occipital face area (OFA) analyses facial parts and the fusiform face area (FFA) engages in more holistic processing of the face)^{1,5–7}, whereas more anterior regions, such as the anterior temporal lobe (ATL) and amygdala (AMG), link faces to conceptual knowledge and affective states^{8–11}. Other regions that appear to have a role in face processing include the posterior superior temporal sulcus (STS), which is involved in processing facial movements^{5,12}; the posterior cingulate cortex (PCC), which is potentially involved in episodic memory related to faces⁶; the inferior frontal gyrus (IFG), which mediates emotion and gaze perception^{13,14}; and the orbitofrontal cortex (OFC), which is thought to evaluate socially rewarding aspects of faces such as their attractiveness and trustworthiness^{15–19}.

How these regions are interconnected and how they functionally interact to give rise to the detailed perceptual, social, affective and mnemonic abilities that constitute face processing is poorly understood. One highly influential model of face processing—the Haxby model^{5,6,20}—postulates a serial-hierarchical structure in which information flows from face patch to face patch in an orderly manner, from posterior brain regions to anterior regions (for example, the OFA to FFA; OFA to STS). Furthermore, this model claims that

there is a unique face processing core system—the OFA, FFA and STS—that performs the most important aspects of face processing while the extended system—the ATL, AMG and PCC—gleans other information from faces. More recent models have extended the Haxby model by suggesting that there are two face processing streams—a dorsal stream and a ventral stream—and that there is some reciprocal processing within each stream^{1,7,21}.

Initial research into how face-sensitive regions are interconnected has primarily implicated portions of a large white matter tract that runs along the ventral visual stream, the inferior longitudinal fasciculus (ILF) in face processing²². However, these studies were limited because they relied on small sample sizes and they examined partial connectomes; links to behavioural performance are often lacking and they did not investigate structural connectivity (SC) and functional connectivity (FC) or effective connectivity (EC) together^{23–26}. It remains unclear how the full set of face-sensitive regions is anatomically interconnected, how they functionally interact with each other across tasks and contexts and how network-level characteristics relate to behaviour.

Here we tested predictions of prominent neurocognitive models of face processing^{1,5,6,20} as well as asking several new questions derived from anatomy studies about the role of short-range versus long-range white matter, and tested an older idea about the possible genesis of hemispheric asymmetries in face processing. We used the human connectome project (HCP)²⁷ dataset because it provides a large population of individuals and high quality multimodal neuroimaging data. We functionally defined nine face-sensitive regions in each individual, then used tractography to delineate local, long-range and cross-hemisphere white matter connections. We also investigated functional and dynamical properties of this network using paired resting-state and task-state functional datasets, and we explored the anatomy–function relationship by studying the correspondence between anatomical and functional connectomes. Finally, we used HCP behavioural tests to examine whether individual differences in certain face skills (such as facial emotion recognition) can be explained by any connectome characteristics.

¹State Key Laboratory of Cognitive Neuroscience and Learning, and IDG/McGovern Institute for Brain Research, Beijing Normal University, Beijing, China.

²Department of Psychology, Temple University, Philadelphia, PA, USA. ³Department of Psychology, Drexel University, Philadelphia, PA, USA. ⁴Department of Neurology, Perelman School of Medicine, University of Pennsylvania, Philadelphia, PA, USA. ⁵School of Psychological and Cognitive Sciences and Beijing Key Laboratory of Behavior and Mental Health, Peking University, Beijing, China. ⁶These authors contributed equally: Yin Wang, Athanasia Metoki.

*e-mail: mirrorneuronwang@gmail.com; iolson@temple.edu

Results

Anatomical connectome. Diffusion MRI (dMRI) combined with tractography is, at present, the only in vivo method that can be used to delineate the fibre tracts between brain regions. Tractography obtains diffusion measurements as input and produces the connectome, which is a collection of white matter fascicles, as output²⁸. Tractography is not without its limitations^{29,30}, but several examples to date have demonstrated that the results of tractography correlate well with the results from histology^{31–33}. Using five independent but complementary tractography analyses, we obtained a detailed and comprehensive picture of the face network structural connectome.

First, we mapped the global connectivity pattern for each face region of interest (ROI). Axonal projections determine where a region receives information from and where it can exert effects. Although the major cortical projections of each face ROI were its neighbouring areas, they exhibited idiosyncratic distant projections (Supplementary Fig. 1). Posterior areas (OFA and FFA) had large projections to the temporal pole along the ventral temporal cortex. By contrast, the STS had prominent projections in and around the IFG, and vice versa. Medial ROIs (AMG, OFC and PCC) had projections only to medial structures. Furthermore, most face ROIs seemed to have direct fibre projections from the early visual cortex (EVC).

The global connectivity patterns also implied that each region might have differential cross-hemispheric projections to its counterpart in the other hemisphere (different corpus callosum projections from each face ROI are provided in Supplementary Fig. 1). To further examine this, we reconstructed interhemispheric connections for each pair of bilateral ROIs (for example, Left FFA with right FFA). The results confirmed our speculation by showing that bilateral face ROIs were mainly connected through four different midline structures (Extended Data Fig. 1)—the rostrum (OFC), the genu (IFG) and the splenium (OFA, FFA, STS, PCC and ATL) of the corpus callosum, and the anterior commissure (AMG and ATL).

We next delineated inter-regional connections between face areas within the same hemisphere. Anatomical connection strength is often interpreted as a measure of capacity for information flow and provides insights about key pathways through which neural signals propagate within the network³⁴. Here we reconstructed 36 pairwise connections between nine face ROIs in each hemisphere and extracted their microstructural properties (such as connectivity probability and streamline counts) to estimate SC. The landscape of the connectivity probability map (Fig. 1a) indicated that there were three core pathways in the face network: a ventral pathway (EVC–OFA–FFA–ATL–AMG), a medial pathway (AMG–OFC–PCC) and a dorsal pathway (STS–IFG). A similar pattern was also found in the streamline count map (Supplementary Fig. 2). To further validate this partition of three core pathways, we examined another established graph theoretic measure, the communicability, between each ROI pair³⁵. In contrast to the connection weight between a pair of regions (which only measures the direct path), communicability quantifies the ease of communication through all of the possible paths between regions by taking into consideration both direct and indirect connections. Communicability therefore encodes additional useful information about the global organization of a network that mediates inter-regional communication and has been widely used to determine anatomical communities³⁶. Here the community detection analysis on the communicability graph confirmed the existence of three separate communities in the face network and they corresponded well with the partitions of three core pathways (Fig. 1b).

How are these core pathways formed? One possibility is that they are constructed from large white matter bundles such as major fasciculi. Indeed, a small number of long-range tracts has been repeatedly reported in the face-perception literature and disruption of these tracts can lead to prosopagnosia²². Here we used an automatic

fibre reconstruction technique³⁷ to delineate ten major fasciculi for each individual and compared them with the ROI–ROI tracts at the individual level. By calculating the degree of their overlapped trajectories, we estimated the involvement of major fasciculi in the face connectome. The results revealed that the three core pathways were mainly supported by six major fasciculi, but to a much lesser degree than we expected (Fig. 2). Specifically, less than 30% of the ventral pathway was mediated by the ILF ($28.79 \pm 8.11\%$ (mean \pm s.d.)) and inferior fronto-occipital fasciculus (IFOF, $20.76 \pm 12.27\%$); only around 12% of the medial pathway overlapped with the cingulum (CING, $15.03 \pm 10.24\%$) and uncinatus fasciculus (UF, $8.96 \pm 6.58\%$); less than 30% of the dorsal pathway was found to be merged with the arcuate fasciculus (AF, $29.05 \pm 9.15\%$) and superior longitudinal fasciculus (SLF, $25.01 \pm 7.46\%$).

As only a small proportion of the anatomical connectome was contributed by major fasciculi, we directed our attention to another important class of white matter—short-range or U-shaped fibres. Tracer studies have demonstrated that long-range fasciculi comprise only a minority of the whole brain connectome; the majority of the brain connectome consists of short association fibres that lie immediately beneath the grey matter, connecting adjacent gyri^{38–40}. By projecting all 72 ROI–ROI connections over two standard white matter atlases of long-range⁴¹ and short-range fibres^{42,43}, we examined the relative contribution of the two white matter systems for the face connectome (Fig. 2). Although more than 57.0% of the ROI–ROI connections can be classified as short-range fibres, only 34.3% of the connectome can be labelled by the tracts in the long-range white matter atlas. We also found a positive relationship between the spatial distance of two ROIs and the contribution of long-range fibres (Pearson's $r_{72} = 0.314$, $P = 0.007$, 95% confidence interval (CI) = 0.088–0.540), suggesting that greater separation between two face ROIs (for example, EVC–OFA versus EVC–OFC) is associated with increased involvement of long-range fibres in constructing their connections (for example, 4% versus 45%).

Functional connectome. The anatomical connectome strictly allows some neuronal populations to directly interact while excluding most others. By contrast, the functional connectome is inherently dynamic and context dependent⁴⁴. We mapped three different classes of functional brain connectivity to reveal the manner in which face ROIs interact; coactivation patterns were identified during rest (resting-state FC (rsFC)) or during the face localizer task (task-state FC (taskFC)), and EC was modelled using psychophysiological interaction (PPI) and dynamic causal modelling (DCM) to reveal directional information flow driven by the face stimuli^{45–47}.

We found that the results from the rsFC and taskFC analysis were highly correlated (mean $r = 0.518$, $t_{666} = 80.97$, $P < 0.001$, Cohen's $d = 4.43$, 95% CI = 0.505–0.531; Fig. 3f), consistent with recent findings from the connectome at large^{48,49}. Both showed strong coactivations among six face ROIs (EVC, OFA, FFA, STS, IFG and PCC; Fig. 3c,d). This suggests that an intrinsic functional subnetwork exists within the face system that is constantly active and synchronized across contexts^{44,48,50}. However, FC only expresses statistical dependencies (correlations) among time courses that do not generally represent direct neuronal signalling³⁴. By contrast, EC has been proposed as a more powerful route to capture stimulus-driven patterns of directional influence among neural areas⁵¹. Here we implemented PPI to explore network-level dynamics evoked by face stimuli and then used DCM for confirmatory analyses. PPI analyses build simple static models of coupling between one or more brain regions and enable researchers to explore directed changes in connectivity by establishing a significant interaction between the seed region and the psychological context^{51–53}, whereas DCM is a framework for testing alternative hypotheses/models of neural dynamics, fitting them to data and comparing their evidence using Bayesian model comparison^{47,54}. Our PPI analyses revealed that face-sensitive brain dynamics

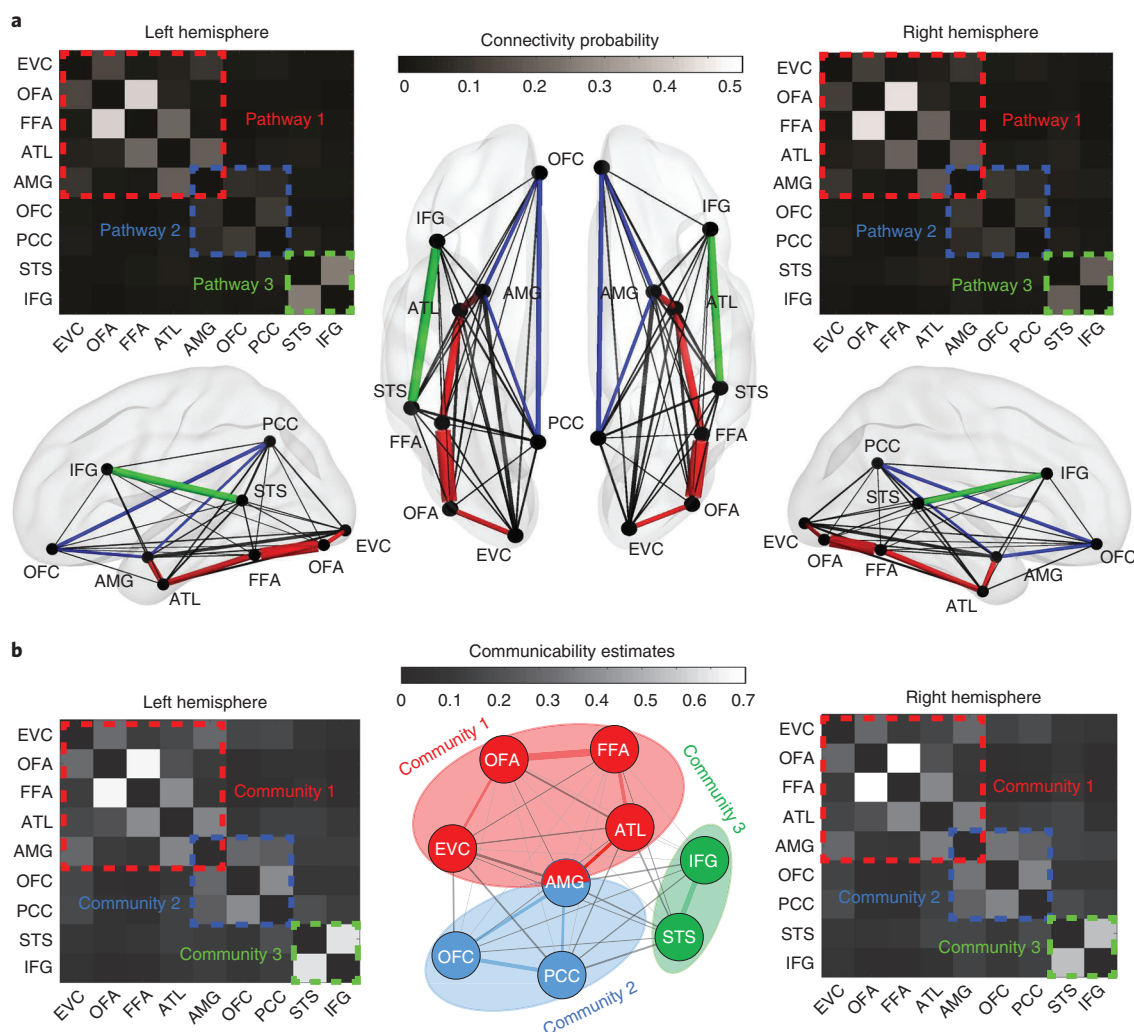


Fig. 1 | The anatomical connectome of the face network. a, The SC map for each hemisphere. The pairwise connection strength (that is, connectivity probability) between nine face ROIs was plotted in weighted matrices and wiring diagrams. The width of each line in the wiring diagrams proportionally reflects the mean connectivity probability across all individuals. The three coloured dashed rectangles indicate three core pathways: EVC–OFA–FFA–ATL–AMG (pathway 1, red), AMG–OFC–PCC (pathway 2, blue) and STS–IFG (pathway 3, green). **b**, The communicability map for each hemisphere. On the basis of graph theory, we derived the communicability map from the SC matrix of individuals (see Methods). Subsequent community detection analysis (middle) indicated three communities within the face network: EVC–OFA–FFA–ATL–AMG (community 1, red), AMG–OFC–PCC (community 2, blue) and STS–IFG (community 3, green). We found that AMG was shared by communities 1 and 2. The three communities found in the communicability graph resonated well with the partitioning of the three core pathways in the SC graphs.

primarily occurred to the same functional subnetwork (Fig. 3e) but with entirely different patterns between the two hemispheres (Fig. 4). Although information processing within the left hemisphere was organized in a purely feedforward manner (that is, the information cascade unfolded from posterior to anterior ROIs), the right hemisphere exhibited a predominantly recurrent architecture (that is, reciprocal connections). For example, multiple bidirectional effective connections were observed among right core face areas (EVC, OFA, FFA and STS; Fig. 4), suggesting the coexistence of bottom-up and top-down interactions and computations during face viewing. Critically, this differential pattern across the two hemispheres was supported by subsequent DCM analyses (Fig. 4b). Results from the Bayesian model comparison suggest that the feedforward processing model fits best with the data observed in the left hemisphere, whereas the recurrent processing model fits best for data in the right hemisphere. For Bayesian model selection (BMS) fixed-effects and random-effects analysis, the feedforward model exhibited higher group log-evidence (619.04 versus 1.12) and exceedance probability

(99.83% versus 0.17%) than the recurrent model in the left hemisphere, whereas the recurrent model exhibited higher group log-evidence (65.39 versus 0.84) and exceedance probability (91.21% versus 8.79%) than the feedforward model in the right hemisphere. An analysis of absolute model fit suggests that the feedforward model can explain $16 \pm 8\%$ (mean \pm s.d.) of the observed variance in the left hemisphere and the recurrent model accounts for $18 \pm 9\%$ of the observed variance in the right hemisphere. An additional DCM analysis with larger model space was also performed to revalidate this differential pattern of face-evoked information processing across two hemispheres (Extended Data Fig. 2).

Spatial specificity of the face connectome. It is important to consider whether the brain connectivity patterns that we observed demonstrate spatial specificity (Fig. 5). On the basis of individual-specific ROIs defined by the face localizer, we discovered three distinct pathways in the anatomical connectome and six synchronized areas in the functional connectome (Fig. 3). To further explore how

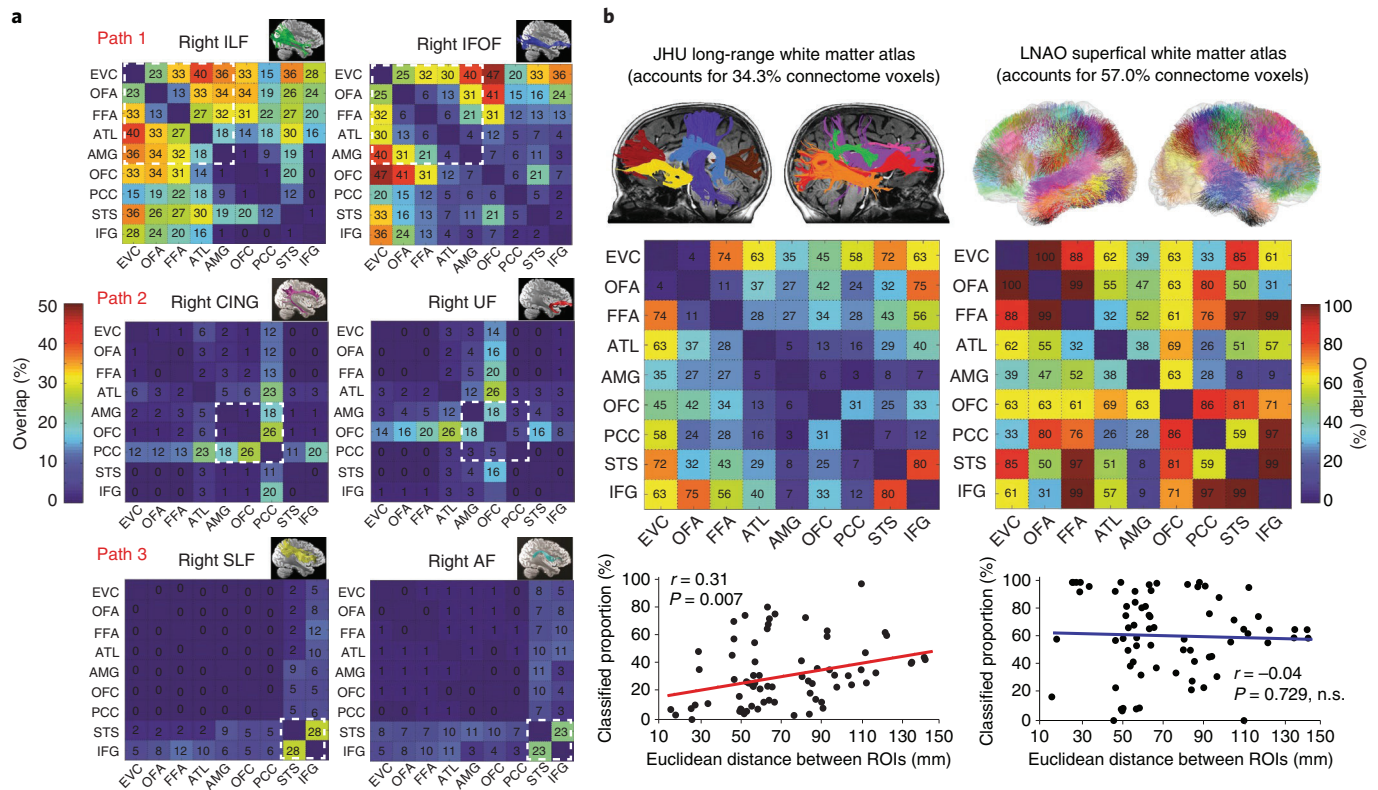


Fig. 2 | The relative contribution of long-range and short-range fibres to the face connectome. **a**, The overlap between six major white matter bundles³⁷ and the face connectome in the right hemisphere. Each percentage value in the matrices represents the mean overlapped volumes between an ROI-ROI connection and a major fasciculi across all individuals. Taking the FFA-ATL connection as an example, 27% voxels of the tract overlapped with the ILF and 6% overlapped with the IFOF; the tract did not overlap with the SLF (0%) and had a minimal portion of overlap with the CING (2%), UF (2%) and AF (1%). After reviewing all of the overlap maps with ten major fasciculi in the right hemisphere, we found that the primary contributors to the ventral pathway (EVC-OFA-FFA-ATL-AMG) were the ILF and IFOF, the medial pathway (AMG-OFC-PCC) was mainly constructed with the UF and CING, and the dorsal pathway (STS-IFG) was mostly supported by the SLF and AF. Similar results were found in the left hemisphere (Supplementary Fig. 3). **b**, After overlaying all 72 ROI-ROI connections (across two hemispheres) onto two standard white matter atlases, we found that around 57% of the face connectome can be classified as short-range fibres, whereas only approximately 34.3% can be labelled as long-range fibres. For each ROI-ROI connection, the values in the matrices represent how well the connection can be explained by the tracts in each atlas. In the OFA-FFA connection, for example, 11% of voxels in bilateral OFA-FFA connections overlapped with long-range tracts in the JHU atlas⁴¹, whereas 99% of voxels in bilateral OFA-FFA connections overlapped with superficial tracts in the LNAO atlas⁴³. Results for each hemisphere are provided in Supplementary Fig. 4. Moreover, we found an important relationship between the face connectome and the long-range fibres: the farther two face ROIs were spatially separated from each other (for example, EVC-OFA versus EVC-OFC), the more contributions long-range fibres made to their connections (for example, 4% versus 45%). No credible evidence of such linear relationship was found for short-range fibres ($r = -0.042$, $P = 0.729$, $BF_{10} = 0.098$). Top left image adapted from ref. ³⁷; top right image reproduced from ref. ⁴³.

these connectivity organizations are spread and changed in space, we performed analogous tractography and connectivity analyses while using two other methods to select the locations of ROIs. When we shuffled individual-specific ROIs across individuals (so that the OFA coordinates of individual A became the OFA coordinates of individual B), we found that the shuffled maps remained almost the same as the original ones for SC ($r_{36} = 0.995$, $P < 0.001$, 95% CI = 0.961–1.029), rsFC ($r_{36} = 0.991$, $P < 0.001$, 95% CI = 0.944–1.038) and taskFC ($r_{36} = 0.987$, $P < 0.001$, 95% CI = 0.930–1.043), but the EC pattern was substantially altered after this permutation manipulation (that is, the shuffled and original EC maps were no longer correlated; $r_{72} = -0.091$, $P = 0.445$, 95% CI = -0.329–0.146; Jeffreys-Zellner-Siow Bayes factor (BF_{10}) = 0.124; Fig. 5, middle row). When we moved each ROI farther away from its putative range (for example, 20mm apart from its original coordinates), we found that the topologies of all brain connectivity were completely changed (that is, the 20mm shifting maps were no longer correlated with original ones; for SC: $r_{36} = 0.231$, $P = 0.175$, 95% CI = -0.108–0.570, $BF_{10} = 0.323$; for rsFC: $r_{36} = 0.241$, $P = 0.156$, 95% CI = -0.097–0.579, $BF_{10} = 0.351$; for taskFC: $r_{36} = 0.113$, $P = 0.510$,

95% CI = -0.233–0.460; $BF_{10} = 0.161$; for EC: $r_{72} = -0.191$, $P = 0.109$, 95% CI = -0.425–0.043; $BF_{10} = 0.334$; Fig. 5, bottom row). These findings suggest that the intrinsic architectures of the face network (that is, SC, rsFC and taskFC) might follow a more global pattern that is configured as relatively stable across small spatial extent (for example, <15 mm), and face-sensitive voxels and nearby non-face-sensitive voxels share similar fibre tracts and, therefore, exhibit resembled neural signal propagations. By contrast, the dynamic features of the face connectome (that is, EC pattern) seem to be highly determined by the voxel-level face selectivity.

Individual variance of the face connectome. It is also important to consider the similarity of face-network organization across individuals. As Fig. 3 shows only group-averaged brain connectivity maps, we would like to validate how representative these group-averaged maps were. To reveal the distribution of group-to-individual similarity across all of the individuals, we conducted correlation analyses between group-averaged maps and individual-specific maps for each type of brain connectivity measure (Supplementary Fig. 6a). The results suggested that

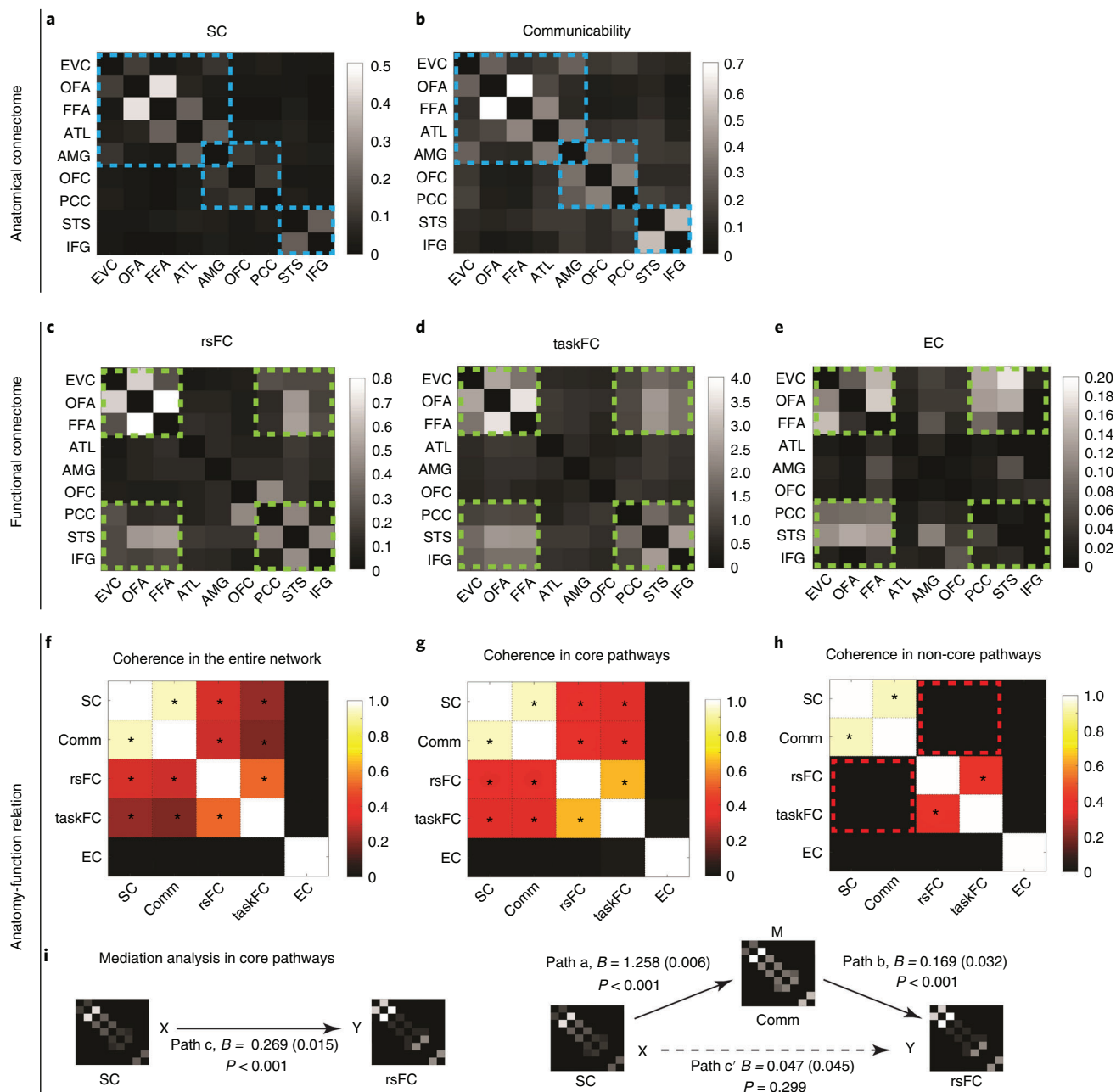


Fig. 3 | All of the brain connectivity maps of the face network and their correspondences. **a, b**, The anatomical connectome, consisting of three core pathways and communities (highlighted by blue dashed lines). **c–e**, Functional brain connectivity patterns during rest or during the face localizer task. Most co-activations (**c** and **d**) and task-modulated brain dynamics (**e**; from PPI analyses) were observed among six face areas (that is, EVC, OFA, FFA, PCC, STS and IFG, which are highlighted by green dashed lines). **f–i**, The correspondence between different types of brain connectivity, either across the entire network or only within the three core pathways. Comm, communicability. For **f, g** and **h**, asterisks indicate significant positive correlations between two connectivity types. The results in **f** show that the SC (**a**) and communicability (**b**) maps across the entire face network were highly correlated with FC maps (rsFC (**c**) and taskFC (**d**)), but the EC map (**e**) was dissimilar to any of them, because it reflects asymmetrical and directional information processing during face perception. We further demonstrated that the tight anatomy–function relationship across the entire network was mainly driven by core pathways (**g**) because little evidence of such anatomy–function association was found outside of the core pathways (**h**; the red dashed boxes represent the null anatomy–function correspondence). For simplicity, all of the maps from **a–h** were results from the right hemisphere. The left hemisphere yielded a very similar pattern of correspondence (Supplementary Fig. 5). **i**, Mediation analyses revealed the network communicability functions as mediator for the association between anatomical connectivity and FC. This mediator role was only found in the core pathways (but no evidence was found for the entire face network). The values in brackets indicate the standard error of the coefficient in each mediation model.

group-averaged matrices were strongly correlated with individual-specific matrices for SC, rsFC and taskFC (Supplementary Fig. 6a), and most individuals (>75%) exhibited maps that were highly similar ($r > 0.5$) to the group-averaged maps. However, the

group-averaged EC matrices showed moderate correlation with individual-specific EC matrices, and most individuals (>67%) exhibited small-to-medium correlation ($0.1 < r < 0.5$) with the group-averaged matrices.

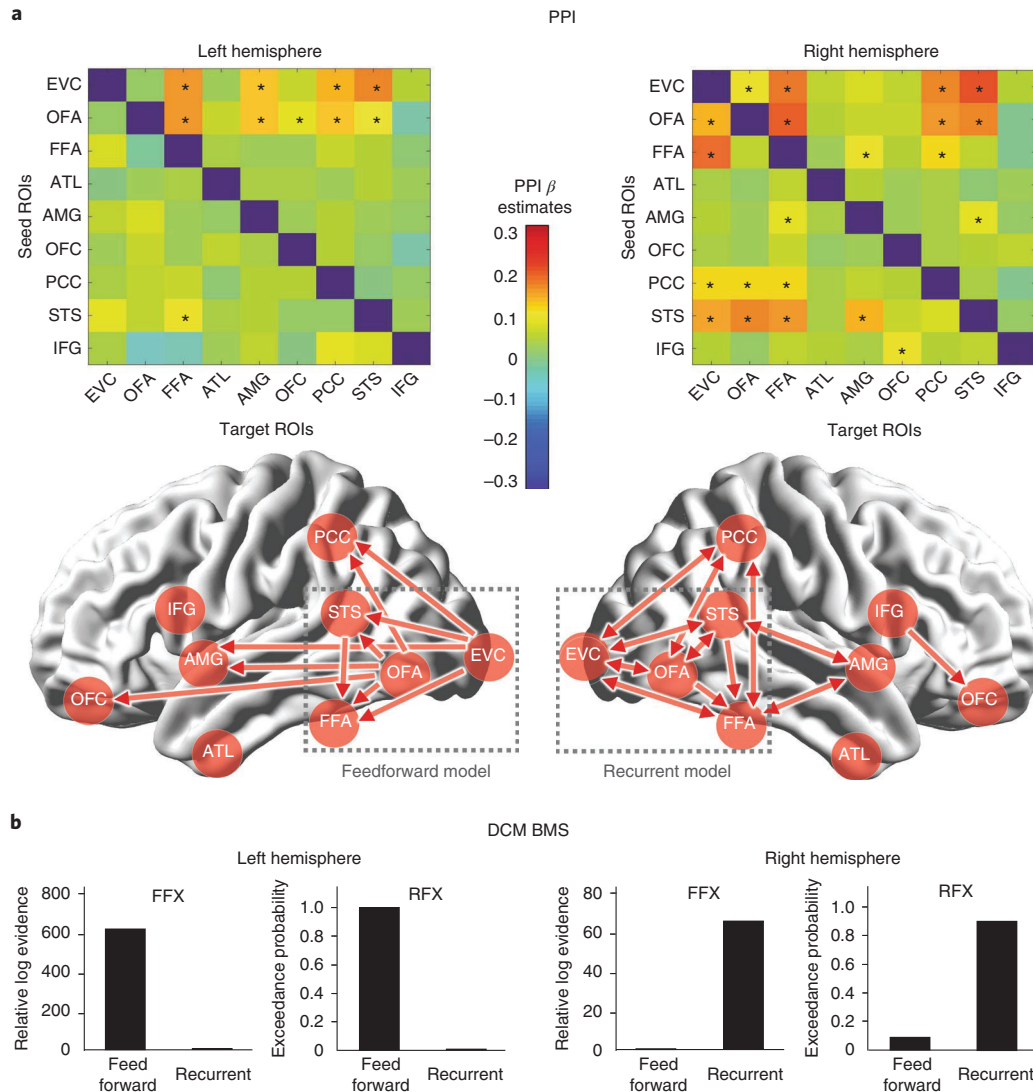


Fig. 4 | The brain dynamics within the face network during the face localizer task. a, PPI results. Top: EC matrices for each hemisphere. The asterisks indicate statistically significant EC. Bottom: an illustration of all directional information flow summarized from the two EC matrices. Qualitatively, the two hemispheres exhibited entirely different patterns of brain dynamics. Only feedforward information cascades were identified in the left hemisphere, whereas both feedforward and feedback processing were found in the right hemisphere. To further validate these PPI findings, we built two DCM models (that is, feedforward versus recurrent) and tested their respective fitness to the observed data in each hemisphere. As the most powerful applications of DCM used networks with a relatively small number of nodes and a relatively simple model space motivated by a priori knowledge, the two DCM models were constructed with four core face areas that interacted in the same way as in the PPI results (the two dashed grey boxes). Further details of model specifications as well as additional exploratory analysis of a larger model space are provided in Extended Data Fig. 2. **b**, DCM BMS results. The fixed-effects (FFX) and random-effects (RFX) group analyses consistently indicated that the feedforward model was optimal for the left hemisphere, whereas the recurrent model was optimal for the right hemisphere. Overall, the EC analyses using PPI and DCM both suggested a differential pattern of face-evoked information processing across two hemispheres.

Next, we used two cross-validation schemes to further study group-to-group and group-to-individual similarity, that is, the split-half cross-validation (using matrices of 50% of individuals to predict matrices for the other 50% of individuals) and the LOOCV (using matrices of $n - 1$ individuals to predict the matrices of a new individual; Supplementary Fig. 6b). Again, both methods revealed very high train-test correlation for SC, rsFC and taskFC and relative moderate train-test correlation for the EC (Supplementary Fig. 6b). In summary, we found that the organization of the face connectome is highly homogeneous across individuals and, in particular, for SC, rsFC and taskFC. Thus, our reported group-averaged matrices indeed reflect the connectivity patterns of most individuals.

The relationships between SC and FC. To further explore the anatomy-function relationship within the face network, we examined the correspondence between the anatomical and functional connectome. Across the entire network, FC patterns (rsFC and taskFC) were highly correlated with SC and communicability patterns (Fig. 3f; rsFC and SC: mean $r = 0.321$, $t_{666} = 43.72$, $P < 0.001$, $d = 1.69$, 95% CI = 0.306–0.335; rsFC and communicability: mean $r = 0.304$, $t_{666} = 47.42$, $P < 0.001$, $d = 1.84$, 95% CI = 0.291–0.316; taskFC and SC: mean $r = 0.234$, $t_{666} = 33.73$, $P < 0.001$, $d = 1.31$, 95% CI = 0.221–0.248; taskFC and communicability: mean $r = 0.199$, $t_{666} = 32.50$, $P < 0.001$, $d = 1.26$, 95% CI = 0.187–0.211). This supports the idea that FC is dictated by the underlying white matter architecture and network communicability^{34,55}. However, when we

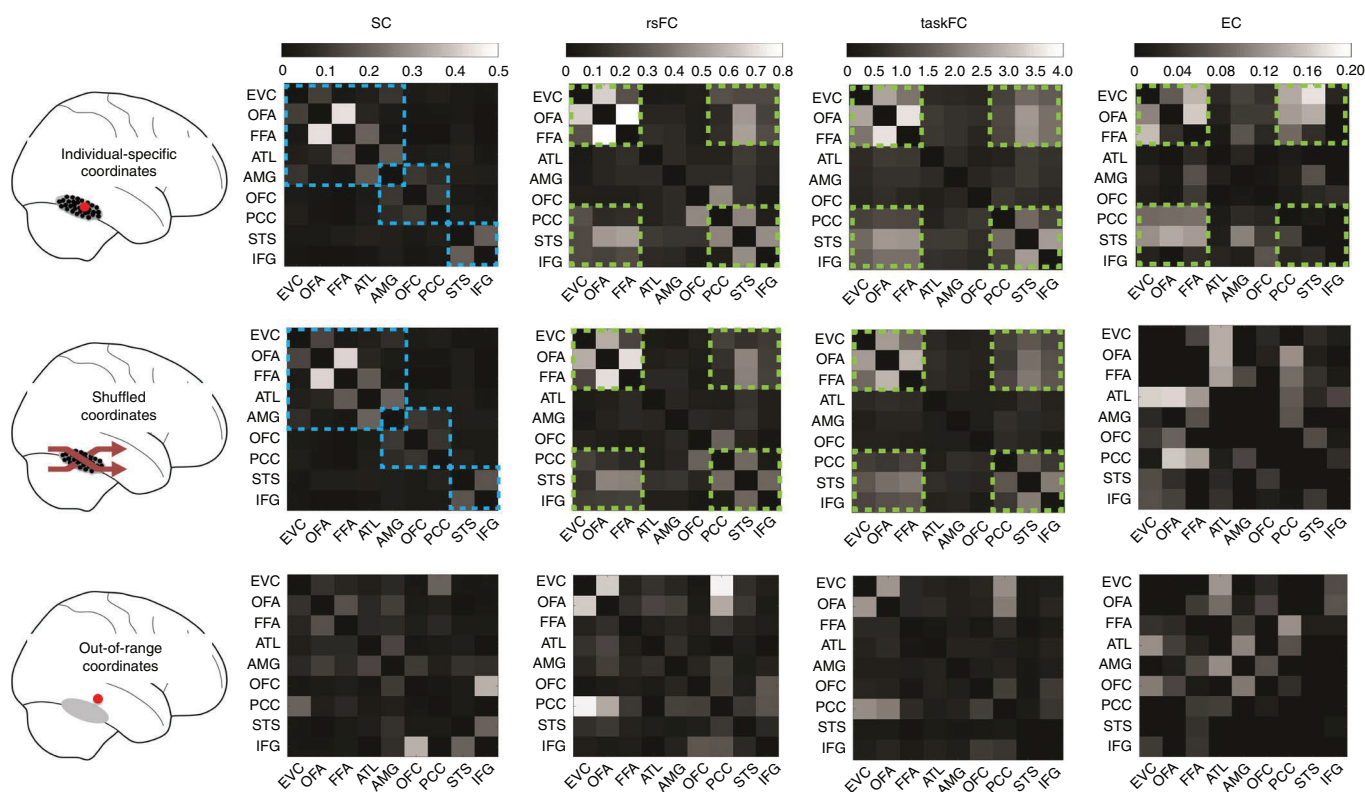


Fig. 5 | The spatial specificity of face connectome organizations in the right hemisphere. Brain connectivity patterns were measured and compared across three different methods of defining ROIs. Top row: we first defined each ROI using individual-specific coordinates from the functional face localizer. The major findings in this Article were obtained using this method, such as the three distinct pathways found in the SC (blue dashed line) and the six synchronized areas found in the FC and EC (green dashed line). Middle row: we then permuted individual-specific coordinates across individuals (for example, the FFA coordinates of individual A now became individual B's; the ATL coordinates of individual C now became individual D's). As the individual variations in the coordinates of each ROI can be typically circumscribed by a sphere with a radius of 10–15 mm (group coordinate ranges are provided in Supplementary Table 1), these new shuffled coordinates were in relatively close proximity to the original individual-specific coordinates. We found that the patterns of SC and FC during rest and task remained the same after this permutation manipulation, but the effectivity connectivity was changed significantly. Bottom row: finally, we chose new ROIs even farther away in space—with new coordinates just outside the putative range (that is, 20 mm from its original coordinates, so that the FFA coordinates of individual A could now fall into the inferior temporal gyrus). After this 20-mm shifting manipulation, these out-of-range coordinates substantially altered all four brain connectivity patterns, therefore showing that our findings had spatial specificity. Similar results of spatial specificity were found in the left hemisphere.

scrutinized the anatomy–function similarity inside or outside the core pathways, we observed this tight relationship in only core pathways (rsFC and SC: mean $r = 0.358$, $t_{666} = 26.46$, $P < 0.001$, $d = 1.02$, 95% CI = 0.331–0.384; rsFC and communicability: mean $r = 0.367$, $t_{666} = 30.21$, $P < 0.001$, $d = 1.17$, 95% CI = 0.343–0.391; taskFC and SC: mean $r = 0.343$, $t_{666} = 25.92$, $P < 0.001$, $d = 1.00$, 95% CI = 0.317–0.369; taskFC and communicability: mean $r = 0.335$, $t_{666} = 27.56$, $P < 0.001$, $d = 1.07$, 95% CI = 0.312–0.359; Fig. 3g) and did not observe statistically significant association in the non-core-pathways (rsFC and SC: mean $r = 0.005$, $t_{666} = 0.72$, $P = 0.473$, $d = 0.03$, 95% CI = -0.009 – 0.020 , $BF_{10} = 0.040$; rsFC and communicability: mean $r = 0.007$, $t_{666} = 0.72$, $P = 0.472$, $d = 0.03$, 95% CI = -0.012 – 0.025 , $BF_{10} = 0.040$; taskFC and SC: mean $r = 0.003$, $t_{666} = 0.36$, $P = 0.722$, $d = 0.01$, 95% CI = -0.012 – 0.018 , $BF_{10} = 0.033$; taskFC and communicability: mean $r = 0.004$, $t_{666} = 0.44$, $P = 0.659$, $d = 0.02$, 95% CI = -0.015 – 0.023 , $BF_{10} = 0.034$; Fig. 3h). This suggested that the high anatomical–function coherence across the entire face network was mainly driven by the core pathways. Furthermore, even though the general pattern of SC and FC were highly correlated inside the core pathways, strong disagreement was observed in multiple connections (Fig. 3a,c). For example, we found that the FFA and ATL are structurally interconnected but are not functionally interconnected (the same applies to ATL–AMG). By contrast, the

OFA–STS and FFA–STS showed strong FC but weak SC. All of these observations suggest that rsFC is an imperfect representation of the underlying SC^{56,57}.

Previous research reported that communicability might be a useful analytical measure to link SC and FC^{58,59}. To test this hypothesis, we applied multilevel mediation analyses to our data, assessing whether communicability mediated the relationship between SC and rsFC. For the core pathways (Fig. 3i), the results showed that SC significantly predicted rsFC (path c: unstandardized beta (B) = 0.269, s.e. = 0.015 $P < 0.001$), which was consistent with our correlation analysis in Fig. 3g; however, after adding communicability into the model, we found no statistically significant association between SC and rsFC (path c': $B = 0.047$, s.e. = 0.045, $P = 0.299$). Moreover, as assessed using Akaike's information criterion (AIC) and Bayesian information criterion (BIC), model fit was greater with communicability added in as the mediator (AIC = 1,211.84; BIC = 1,271.08) compared with the model in which SC independently predicted rsFC (AIC = 1,230.10; BIC = 1,289.33), indicating that communicability fully mediated the relationship between SC and rsFC. By contrast, no credible evidence suggests that communicability is a mediator between SC and rsFC for the entire face network (path c: $B = 0.220$, s.e. = 0.008, $P < 0.001$, AIC = $-15,981.75$, BIC = $-15,340.85$; path c': $B = 0.279$, s.e. = 0.022, $P < 0.001$,

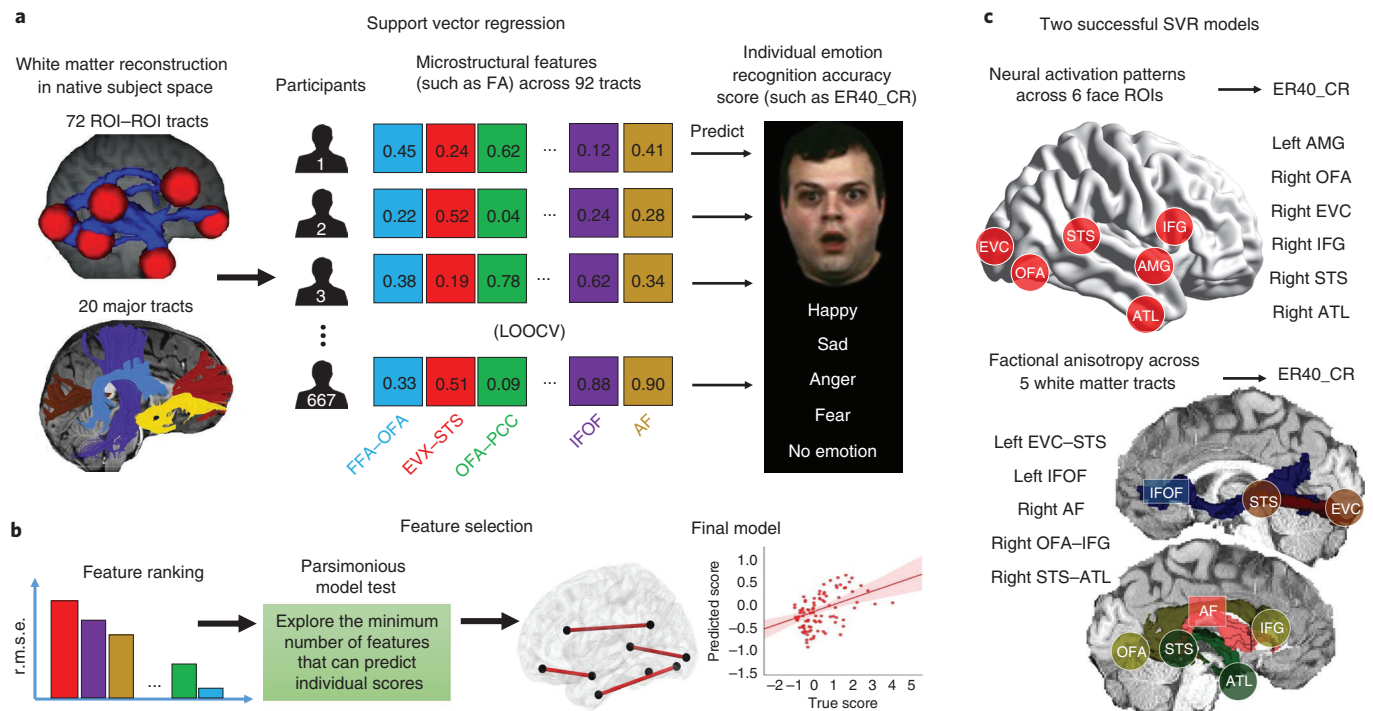


Fig. 6 | Schematic overview of the methods and results used in the brain-behaviour association. **a**, For each group of brain metrics (such as neural activity, white matter characteristics, FC or effectivity connectivity), we built a separate model for SVR. For example, for the white matter FA, we extracted FA values from 92 white matter tracts (72 ROI-ROI connections + 20 major fasciculi) across all of the individuals and set them as independent features in the model. We adopted a leave-one-individual-out cross-validation (LOOCV) scheme to train and test data and examined whether the SVR model of a particular brain metric (such as FA) can predict a performance score (such as emotion recognition accuracy, ER40_CR (ref. ¹⁰¹)). If the predicted score was significantly associated with the true score, we proceeded to the feature selection step. Image of male's face reproduced from ref. ¹⁰¹ with permission (Elsevier). **b**, We used a leave-one-feature-out method for feature selection (with a fivefold cross-validation scheme) and ranked the importance of each feature on the basis of the incurred r.m.s.e. in the absence of that feature. We next performed the parsimonious model test by sequentially testing a series of SVR models with combination of top n important features (for example, top 10 at first, then top 9, 8, 7, and so on) until we had a model with $n - 1$ features that was no longer able to predict the performance of an individual. Again, we adopted the LOOCV scheme to train and test data in the parsimonious model test. **c**, Among all of the groups of brain metrics, we found that only the SVM model with neural activity of all the face ROIs and the model with FA value of all tracts can successfully predict the emotion recognition accuracy of an individual. The parsimonious model tests further revealed a subset of six face ROIs and a subset of five white matter tracts that were the most predictive features for the two successful SVM models. Note that these two subsets of face ROIs and white matter tracts corresponded well with each other, suggesting that critical tracts were also connecting critical ROIs.

AIC = -15,982.39, BIC = -15,341.50). In summary, we found that communicability mediated the anatomy-function relationship only in core face pathways and it outperformed the standard SC as a predictor of rsFC.

Brain-behaviour associations. The simplest and most popular method for establishing brain-behaviour relationships is correlation. We first computed simple Pearson correlations between the facial emotion recognition performance of individuals and all types of brain measurements (such as blood-oxygen-level-dependent (BOLD) signals from each face area, white matter characteristics, FC and EC). We found no statistically significant univariate correlation in this whole-connectome search (all r values < 0.065, all P values > 0.092, all BF_{10} values < 0.119).

As this simple correlation method is not robust when studying a complex brain-behaviour association⁶⁰ and can typically incur serious problems of multiple comparison when searching the whole connectome, we subsequently used a machine learning regression algorithm. Individualized behavioural prediction using machine learning regression is becoming increasingly popular in neuroimaging, and this approach has been recommended as multivariate pattern analysis for exploring the complex relationship between behaviour and distributed patterns of brain features^{61,62}. Here we

used support vector regression (SVR) to examine whether the global pattern of any groups of brain metrics can predict individual face processing skills (Fig. 6).

The SVR analyses revealed two groups of brain metrics that can successfully predict individual differences in facial emotion recognition accuracy—the neural activity features from all face ROIs (model goodness-of-fit: adjusted $R^2 = 0.014$, $F_{1,665} = 10.271$, $P = 0.001$, 95% CI = 0.048–0.199) and the fractional anisotropy (FA) profile of all white matter tracts (adjusted $R^2 = 0.016$, $F_{1,665} = 12.136$, $P = 0.001$, 95% CI = 0.058–0.209). To identify the subsets of ROIs or white matter tracts that were essential for prediction, we performed feature selection to rank the contribution of each feature to the SVR model and implemented the parsimonious model test to reveal the minimal subsets that can successfully predict the behaviour. The results revealed a subset of six face ROIs (left AMG, right OFA, right EVC, right IFG, right STS and right ATL) and a subgroup of white matter fibre paths (left EVC-STS, left IFOF, right AF, right OFA-IFG and right STS-ATL) as the most predictive and essential features for the two successful SVR models (Fig. 6c). Notably, the white matter parsimonious model (root-mean-square error (r.m.s.e.) = 0.982) predicted behaviour better than the neural activity parsimonious model (r.m.s.e. = 1.035). To further rule out the possibility that the function of these brain features are only for general

performance (for example, task accuracy and reaction times), we used the two parsimonious models to predict other HCP non-face behavioural performance. We found no credible evidence that these features are predictive of the working memory 2-back task accuracy and speed (that is, neural activity model for accuracy: adjusted $R^2 < 0.001$, $F = 0.57$, $P = 0.450$, 95% CI for $B = -0.047$ – 0.105 , $BF_{10} = 0.041$; neural activity model for speed: adjusted $R^2 = 0.002$, $F = 2.23$, $P = 0.135$, 95% CI for $B = -0.018$ – 0.134 , $BF_{10} = 0.093$; white matter model for accuracy: adjusted $R^2 < 0.001$, $F = 0.09$, $P = 0.770$, 95% CI for $B = -0.065$ – 0.087 , $BF_{10} = 0.032$; white matter model for speed: adjusted $R^2 < 0.001$, $F = 0.03$, $P = 0.859$, 95% CI for $B = -0.083$ – 0.069 , $BF_{10} = 0.031$), theory of mind judgement speed (that is, neural activity model: adjusted $R^2 = 0.001$, $F = 1.89$, $P = 0.169$, 95% CI for $B = -0.023$ – 0.129 , $BF_{10} = 0.079$; white matter model: adjusted $R^2 < 0.001$, $F = 0.01$, $P = 0.911$, 95% CI for $B = -0.072$ – 0.080 , $BF_{10} = 0.031$) and delay-discounting ability (neural activity model: adjusted $R^2 = 0.001$, $F = 1.80$, $P = 0.180$, 95% CI for $B = -0.024$ – 0.128 , $BF_{10} = 0.076$; white matter model: adjusted $R^2 = 0.003$, $F = 3.17$, $P = 0.080$, 95% CI for $B = -0.145$ – 0.007 , $BF_{10} = 0.149$). This confirms that our predictive brain features are specific to face processing. There is little credible evidence that suggests that any FC or EC measures were able to predict accuracy on the facial emotion recognition task (for example, rsFC performance: adjusted $R^2 = 0.002$, $F = 2.24$, $P = 0.135$, 95% CI for $B = -0.018$ – 0.135 , $BF_{10} = 0.094$; EC performance: adjusted $R^2 < 0.001$, $F = 0.01$, $P = 0.931$, 95% CI for $B = -0.079$ – 0.073 , $BF_{10} = 0.031$).

Hemisphere lateralization. Although face processing has been consistently linked to activity in the right hemisphere and unilateral right hemisphere damage can result in prosopagnosia, the same is not true of damage to the left hemisphere¹. Here we investigated whether such lateralization exists at the connectome level. Repeated-measure analysis of variance (ANOVA) revealed significant hemispheric asymmetry in the neural responses of face ROIs ($F_{1,666} = 238.64$, $P < 0.001$, partial $\eta^2 = 0.264$; mean difference = 0.617 , 90% CI = 0.551 – 0.683), white matter connectivity probability ($F_{1,666} = 9.25$, $P = 0.002$, partial $\eta^2 = 0.014$; mean difference = 0.002 , 90% CI = 0.001 – 0.002), rsFC ($F_{1,666} = 17.63$, $P < 0.001$, partial $\eta^2 = 0.026$; mean difference = 0.008 , 90% CI = 0.005 – 0.011) and EC during the face localizer task ($F_{1,666} = 9.17$, $P = 0.003$, partial $\eta^2 = 0.014$; mean difference = 0.023 , 90% CI = 0.011 – 0.036). Post hoc *t*-tests further indicated the direction of lateralization for each condition (Supplementary Table 2). We found that 7 out of 9 face areas showed stronger responses in the right hemisphere; this did not include the EVC and OFC, for which we found no credible evidence of hemispheric difference (EVC: $t = -0.36$, $P = 0.716$, $d = 0.01$, 95% CI = -0.164 – 0.113 , $BF_{10} = 0.033$; OFC: $t = -0.71$, $P = 0.477$, $d = 0.03$, 95% CI = -0.183 – 0.086 , $BF_{10} = 0.028$). For the diffusion-imaging data, mixed results were found in the anatomical connectome; 9 connections lateralized to the right hemisphere (for example, STS, AMG and OFC fibres) and 7 connections lateralized to the left hemisphere (for example, IFG and PCC fibres). We found that 18 connections in the functional connectome exhibited right-hemispheric predominance (9 connections in rsFC and 11 connections in EC), whereas only 2 connections had left-hemispheric predominance (2 connections in rsFC). Importantly, we found a positive correlation between a face area's degree of lateralization and its intra- and interhemispheric connection ratio (Fig. 7); face areas with a high ratio of intra- over interhemispheric connections (for example, STS, OFA, FFA and ATL) exhibited more prominent right hemispheric lateralization in their neural responses to face stimuli ($r_s = 0.769$, $P = 0.015$, 95% CI = 0.197 – 1.340). In summary, we found strong evidence of hemispheric asymmetry at all levels of the face network and face areas in the right hemisphere generally exhibited enhanced neural responses and stronger SC and FC.

Discussion

Here we systematically investigated the anatomical and functional connectome of a well-defined domain-specific system—face processing. Nodes in the face processing network have been rigorously investigated in cognitive neuroscience and neuropsychology for more than 40 years^{1–5}. This literature provides a strong foundation for our network-based analyses that were both hypothesis and data driven, enabling us to explain the mechanisms that underlie face processing at the connectome level.

Our large-scale multi-modal study revealed several interesting findings. First, previous diffusion-imaging studies focused on a subset of face-sensitive regions^{23,24} and proposed the existence of two face processing streams, a ventral pathway for identity processing and a dorsal pathway for processing dynamic aspects of faces^{1,5}. We looked at nine functionally and individually defined face-sensitive regions in each hemisphere, stretching from the occipital lobe to the frontal lobe, and encompassing both core and extended face processing^{1,5,20}. This enabled us to describe segregated pathways of a precise and comprehensive face connectome. The network communicability analysis indicated that the face network can be anatomically divided into three separate pathways: (1) the OFA, FFA and ATL constitute a ventral pathway that possibly extracts static features from faces; (2) the STS and IFG comprise a dorsal pathway, which is specialized for processing dynamic information from faces; and (3) PCC–AMG–OFC form a medial pathway that might be responsible for processing the social, motivational and emotional importance of faces. Multiple medial areas for value and reward processing have been associated with judgements of facial attractiveness and trustworthiness^{10,19,63}. Finally, the ROI-to-ROI tractography patterns showed very weak connection strengths in OFA–STS and FFA–STS, suggesting that they belong to different face processing subsystems, a finding that is consistent with previous diffusion-imaging work^{23,24}.

Second, our results shed light on a disagreement in the literature about the serial and hierarchical nature of the face processing system. An early and prominent model by Haxby et al.⁵ postulated a serial-hierarchical structure, in which the core regions have a strict serial ordering—the OFA feeds into the FFA and STS. More recent human imaging research has modified this scheme by proposing an additional processing node, the ATL, and suggested that the system is recursive⁶⁴. Although some of our data indeed suggest that the OFA, FFA and STS are the most active parts of the face network because they had the largest neural responses to face stimuli and were constantly synchronized during rest and tasks, our overall results challenge these frameworks. The global connectivity patterns demonstrated that the EVC sends projections to most of the face sensitive areas, suggesting that there is no gateway (or solo entry point) for FFA and STS. This is consistent with previous research in patients^{65–67}. Moreover, the dynamic patterns of EC suggest that face processing does not proceed strictly in sequence but, rather, in a parallel and reciprocal manner. Our results are more consistent with research in macaques showing that face patches are densely and bidirectionally interconnected, inconsistent with a serial hierarchy^{3,21}. Importantly, and potentially unique to humans, the two hemispheres appear to perform distinct schemes of computations and interactions during the face localizer task (the left hemisphere is feedforward whereas the right hemisphere is recurrent). Similar functional asymmetries have been reported in face magnetoencephalography studies^{68,69}.

Our third interesting finding is that local white matter has a disproportionate role in the anatomical connectome supporting face processing. On the basis of a recent literature review²², two long-range fibre pathways—the ILF and IFOF—are the most frequently reported tracts associated with face processing (11 out of 16 studies), whereas the local white matter was rarely mentioned (2 out of 16 studies). Moreover, as most face ROIs are spatially far apart (for

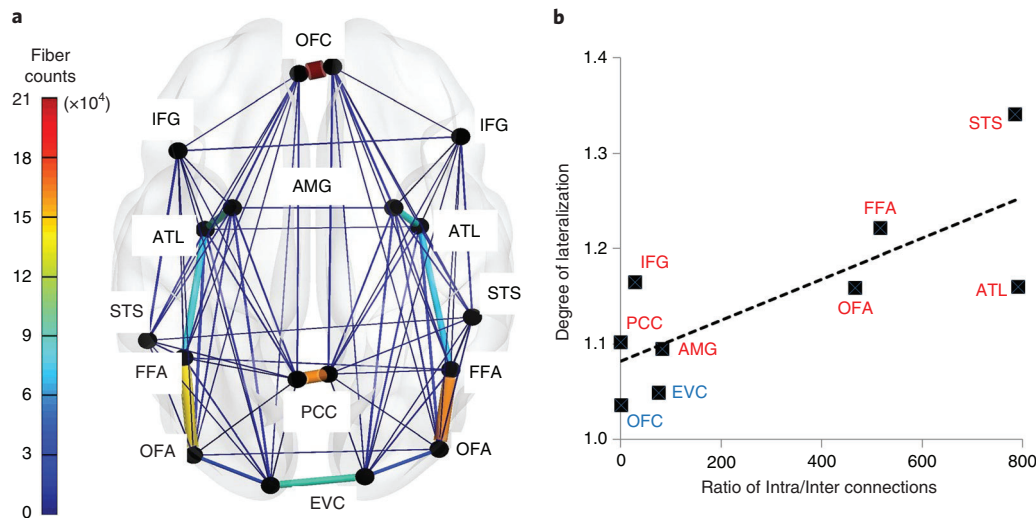


Fig. 7 | The association between the degree of lateralization and the ratio of intra- and interhemispheric connection across all face areas. a, The interhemispheric and intrahemispheric connection strength for each face ROI. The width and the colour of each line in the diagram proportionally reflect mean streamline counts across all of the individuals. **b,** Across all nine face areas, we found a positive correlation between an area's degree of lateralization to face stimuli (y axis, the ratio of BOLD signal magnitude in the right hemisphere node over the left hemisphere node) and its intrahemispheric/interhemispheric connection ratio (x axis; Intra/Inter). Those areas with low ratios of intrahemispheric/interhemispheric connection (such as EVC and OFC) exhibited no lateralization in their neural responses to face stimuli, whereas the areas with high ratios of intrahemispheric/interhemispheric connection (such as STS and FFA) exhibited strong right hemisphere predominance.

example, 75% of connections had a Euclidian distance >50 mm; Fig. 2b), long-range fibres would be expected to play the primary role in the structural connectome. Indeed, our results have shown the incremental proportion of long-range fibres as the distance between two face ROIs increases (Fig. 2b) and there is solid spatial overlap between major fasciculi and three face pathways (that is, the ventral pathway maps onto the ILF and IFOF; the medial pathway was constructed from the UF and CING; and the dorsal pathway consisted of the SLF and AF; Fig. 2a). However, this description of fibre pathways is incomplete because these long-range fibre bundles account for only $\sim 30\%$ of the face connectome. Instead, most face nodes are interconnected by short-range fibres. Our observation is consistent with older histology studies that reported that the human cerebral white matter is dominated by short-range fibres that connect adjacent gyri³⁸ and complies well with the 'small-world' characteristic of brain networks⁷⁰. It is believed that abundant short-range fibres function to adaptively minimize global wiring costs, whereas sparse long-range connections contribute to functional integration^{71,72}. Here we found that most ROI–ROI connections were redundantly constructed from both types of fibres (Fig. 2b), for example, the STS and IFG can be directly linked through major fasciculi (80%) or can be connected indirectly by superficial fibres through multiple-hop-relays (99%). This redundant architecture may provide the face network with resiliency in the case of brain injury and disease, possibly explaining why prosopagnosia is so rare^{64,73}. Future research is needed to explore whether these features (that is, disproportionate local connectivity, distance effect on long-range fibres and redundant connections) are specific to the face network or whether they exist in other domain-specific systems, or can be generalizable to the entire cortical 'neighbourhoods'.

Fourth, we provide empirical evidence of the face processing lateralization at the connectome level. The functional asymmetry of face processing is often referred to as a fundamental lateralization of the human brain⁷⁴. Right hemispheric predominance has been repeatedly found in behavioural performance⁷⁵, neural activation⁷⁶, electrophysiological responses⁷⁷, intracranial stimulation effects⁷⁸ and prosopagnosia cases¹. Compared with the left hemisphere, face

areas in the right hemisphere were more anatomically connected, more synchronized during rest and more actively communicating with each other during face perception. Furthermore, we found a critical association between the ratio of intra- and interhemispheric connection and the degree of lateralization, which lends support to an older theory that suggests that hemispheric asymmetry arises from interhemispheric conduction delay⁷⁹. According to the theory, brain size expansion during evolution led to the emergence of functional lateralization to avoid excessive conduction delays between the hemispheres. This theory predicts that, to function efficiently, functionally lateralized brain regions will have relatively weak callosal connectivity as compared with non-lateralized regions⁸⁰. Our data support this prediction by showing that face areas with stronger functional lateralization exhibited less interhemispheric, but more intrahemispheric, connections. It is plausible that the connectome-level origin of face network lateralization arises from extremely imbalanced intrahemispheric–interhemispheric connections, which causes neural signals to spread more easily among face areas within the same hemisphere than across hemispheres.

We also examined the anatomy–function relationship of the face network by systematically examining relationships between different types of brain connectivity. We found that the topological organization of the anatomical connectome (that is, three core pathways) was consistent across measures (for example, connection probability, communicability and streamline count maps) and the FC patterns were highly similar across resting and task states. This within-modality coherence is in line with reports on other neural networks^{36,48}. We also explored the spatial specificity of all brain connectivity patterns and found that those intrinsic network architectures (that is, SC, rsFC and taskFC) followed a more global pattern that was relatively stable across small spatial scales, whereas the EC pattern seemed to be specific to the face-sensitive sub-regions. However, the relationship between SC and FC is not straightforward. Although the SC and rsFC were globally correlated across the entire network, this effect was mainly driven by high anatomy–function coherence from the core pathways (Fig. 3g), whereas other parts of the network showed no such correspondence (Fig. 3h).

Interestingly, we found a similar ‘global versus local’ discordant pattern in the subsequent mediation analyses in which the communicability fully mediated the prediction from the SC to rsFC in core pathways (Fig. 3i) but not across the entire network. Together, these findings add to a growing body of literature on the complex nature of the anatomy–function relation^{55,81–87} and shed light on why rsFC is an imperfect representation of the underlying neural architecture. Our results demonstrated that, even for a domain-specific system like the face network, the anatomy–function relationship is heterogeneous across different connections and depends highly on the local degree of communicability. Moreover, our data clearly showed that the communicability metric is superior to the SC measure when predicting FC. This is because conventional SC is based on direct connectivity weight but this is too simplistic to model distributed neural communications. The communicability metric takes into consideration all of the direct and indirect relationships between two nodes and, therefore, provides additional information about the global dynamics of the network^{36,59}.

Finally, to explore the brain–behaviour association for individual face skills, we investigated how proficiency of emotion recognition emerges from patterns of neural activity and connectivity among face-sensitive regions. Using multiple SVR analyses, we found that the most predictive brain features for individual performance were distributed across six face-sensitive brain regions and five white matter connections. The HCP emotion recognition test is a complex task that taps into multiple mental constructs and operations (such as perceptual, cognitive, affective and semantic processes). The most predictive brain features corresponded well with the neural bases of these operations—facial identification (EVC, OFA and IFOF), embodied simulation (STS, IFG and AF), affective processing (AMG) and the retrieval of emotion concepts and labels (ATL and STS–ATL)^{22,73,88}. Both hemispheres were probably involved because the task requires face recognition as well as lexical retrieval. Our results accounted for only a small amount of the behavioural variance, potentially due to the fact that the behavioural task is very easy for non-clinical cohorts thereby limiting behavioural variance. However, white matter characteristics outperformed other brain features in individualized behavioural prediction, which signifies that the anatomical connectome is a useful biomarker for individual variation in high-level cognition⁶² and social skills⁷³.

Limitations

This study has some methodological limitations. First, similar to other large-scale publicly available datasets, the HCP has certain inherent problems. For example, the psychometric and neuroimaging data may be suboptimally designed for studying ‘pure’ face processing (for example, the face localizer is embedded in a working memory task and there is only one face-related behavioural test, which is to name emotional faces); the data may therefore contain substantial noise and confounding factors that could in part drive the observed effect^{89,90}. Second, some behavioural tasks (such as the Penn Emotion Recognition Test) were too easy for healthy individuals as they were originally designed for clinical populations, therefore resulting in ceiling effects for brain–behaviour correlation. Furthermore, there is an extremely unbalanced number of right- and left-handed individuals in the HCP dataset (680 versus 70), which prevented us from comparing the face connectome between the two handedness groups (especially for the genesis of hemispheric asymmetries in face processing).

Second, rsFC is prone to methodological and conceptual problems^{91,92}; interpretations should therefore be cautious with regard to their cognitive and causality meanings^{56,81,93}. Moreover, dMRI tractography has recently been criticized for high false-positives and there is an urgent need for methodological innovation in tractography algorithms to address this issue^{29,30,94}. However, these tools provide considerable insights on the structural and functional

architecture of brain networks. As both techniques develop, we hope that other researchers will replicate and extend our findings.

Third, the notion of directionality in PPI is an important topic that often causes confusion. The unidirectional or asymmetric patterns are not uncommon in the PPI literature^{52,53,95} and they were clearly observed in this study (for example, the left hemisphere had only feedforward directions). In a very strict sense, PPI analysis should be interpreted as a simple test for EC because it is based on an explicit (and often linear) model of coupling between one or more brain regions^{45,51}. However, we note that the post hoc interpretation of PPI results can be ambiguous as a significant increase in coupling from one region to another region may be significant when testing for a PPI in the opposite direction⁵². Further research is needed to determine whether the hemispheric differences in information processing observed here are true or an inflated artefact⁹⁶ or are caused by other experimental confounding factors (such as button press by right hand during the task). Furthermore, as DCM is computationally expensive for large data, we only tested few simplistic models with four nodes in this study. Future studies are needed to examine larger model space with other datasets or use other EC approaches^{97–100} to confirm our findings.

Conclusions

Face processing has been investigated in neuroscience research for more than 40 years. Although much research has addressed the functional specialization of single face-selective regions, the connectome-level organization and brain-wide mechanisms for functional integration of face processing remains poorly understood. New trends in connectomics suggest that the function of any face areas should be considered within an integrative approach, including not only patterns revealed by local properties, but also interactions with other face areas⁹⁰. For that, here we used large-scale multimodal neuroimaging data to investigate the anatomical and functional connectome of the face network. Functionally defined white matter tracts, using probabilistic tractography, delineated a well-organized anatomical architecture with three core pathways for different types of information processing. Fibre composition analyses revealed that the anatomical connectome is primarily constructed by short-range fibres, and not major white matter bundles. FC and EC analyses discovered a subnetwork of face areas that are constantly synchronized across contexts and they exhibit differential neural dynamics across hemispheres during face perception (feedforward versus recurrent interactions). Moreover, we found that the SC and FC are highly associated in the face network and network communicability mediates this close correspondence in core pathways. Furthermore, individual differences in face skills can be predicted by a distributed pattern of connectome characteristics, in particular the white matter integrity. Finally, we demonstrate that an imbalanced pattern of intra- and interhemispheric connections might be the connectome-level basis for the hemispheric asymmetry of the face network. Collectively, we discovered a wide range of important features of the face connectome that go beyond the classic as well as more recent models of face processing. These connectome-level characteristics provide new constraints for face-perception theories and offer valuable empirical evidence for a fine-grained organization and interactive mechanisms of face processing.

Methods

Participants. All data used in this study were obtained from the WU-Minn HCP Consortium S900 Release. Individuals were included if they had completed all of the brain scans (T1/T2, task fMRI, resting-state fMRI and dMRI) as well as the behavioural Penn Emotion Recognition Test¹⁰¹. To reduce variance in the human connectome¹⁰², we restricted our population to only to right-handed individuals, resulting in 680 healthy young adults in the final sample (381 females, aged 22–36 years). Only 667 out of 680 individuals were detected with enough robust signals in all nine bilateral face ROIs in the face localizer task (Supplementary Table 1); most of the connectome-level findings were therefore based on 667 individuals. No statistical methods were used to predetermine this sample size, but the sample

size is much larger than those reported in previous publications^{23–26}. The study was reviewed and approved by Temple University's Institutional Review Board.

Data acquisition, preprocessing and analysis. Owing to the complexity of the HCP data acquisition and preprocessing pipeline, listing all of the scanning protocols and data analysis procedures is beyond the scope of this paper; however, the protocols and procedures were described in full detail previously^{27,103–106}. We adopted the 'minimally pre-processed' images of fMRI, rsfMRI and dMRI that were provided by the HCP S900 Release. The dMRI data had been processed for EPI distortion, eddy current and motion correction, gradient nonlinearity correction and registration of the mean b0 volume to a native T1 volume. The fMRI data had undergone spatial artefact/distortion correction, cross-modal registration and spatial normalization to Montreal Neurological Institute (MNI) space. Moreover, we further processed the dMRI data using FSL's BEDPOSTX¹⁰⁷ to model white matter fibre orientations and crossing fibres, and denoised the rsfMRI data using ICA-FIX and fMRI data with ICA-AROMA¹⁰⁸ to remove motion artefacts. All fMRI data were spatially smoothed at 4 mm. Furthermore, to precisely localize each face ROI^{109,110}, the face localizer task was processed on the 'greyordinate-based' space (that is, cortical surface vertices + subcortical voxels) using MSM-All registration¹¹¹.

We used the HCP Penn Emotion Recognition Test as a behavioural measure of individual face recognition ability¹⁰¹. Individuals were presented with 40 faces, one at a time. They were asked to choose what emotion the face depicted: happy, sad, angry, scared or no feeling. Half of the faces were males and half were females. The task overall accuracy (ER40_CR) and median reaction time (ER40_CRT) were used in the brain–behaviour association analyses.

To ensure sensitivity to the connectome within each individual, we not only defined individual-specific ROIs on the basis of the face localizer, but also performed all analyses first at the individual level and then combined them into an aggregate statistic for group-level inference and significance tests. Unless otherwise stated, all significant results reported in this study were two-tailed tests and were false-discovery-rate corrected for multiple comparisons. Data distribution was assumed to be normal but this was not formally tested. Moreover, all of the null results were further evaluated using Bayesian statistics (BF₁₀) in SPSS v.25.

Functional face localizer and selection of face ROIs. The working memory task in the HCP fMRI data can be effectively used as a functional face localizer¹⁰⁵. Individuals were presented with alternating blocks of four categories of stimuli (that is, faces, places, tools and body parts) and were instructed to respond in a manner of 2-back and 0-back tasks. As the HCP S900 release had already provided the individual-level (within-individual) fMRI analysis data that were fully processed on greyordinate space, we used the connectome workbench software to manually extract the vertices (which were later transformed to MNI coordinates) of the peak activation of bilateral nine predefined face ROIs (as well as its magnitude) from the contrast 'faces > other categories' for each individual separately (Supplementary Table 1). This task paradigm and contrast has been widely used to define human face-sensitive areas^{112,113} and the processing for face and working memory are orthogonal to each other in this contrast (that is, face conditions were collapsed across both 0-back and 2-back trials). To ensure the selection of face-sensitive voxels, we also inspected another conjunction contrast ('faces > places' \cap 'faces > tools' \cap 'faces > body parts') and obtained very similar peak coordinates. These individual-specific cluster peak coordinates were used as input (spheres, 6 mm radius) for subsequent seed-based brain connectivity analyses at the individual level (probabilistic tractography, resting-state analysis, PPI and DCM), and the cluster peak magnitudes were adopted as the index of neural activity for face ROIs in brain–behaviour association and hemispheric asymmetry analysis.

As we are interested in the broader face network, we selected areas not only for basic face perception (OFA, FFA and STS), but also for social, emotional and mnemonic processing of faces (ATL, OFC, AMG, IFG and PCC). A similar set of areas was included in the Haxby model^{5,6,20} and these areas were widely used in previous face network studies^{23–26,112}. Moreover, for face areas with multiple clusters (such as OFA, FFA and STS) we simply chose the strongest one to avoid excessive interindividual variability²⁴. We note that some regions that were recently identified in a study of non-human primates, which showed strong connectivity with face patches (for example, the pulvinar and claustrum; Grimaldi et al.²¹), were not selected in our study because they were not consistently activated by our face localizer task and the relevant human literature on these regions is lacking.

Probabilistic tractography. Tractography analyses were performed in the native space of individuals and all of the results were transformed to MNI standard space. We used both a single-ROI and an ROI-to-ROI approach. In the single-ROI approach, each ROI was used as a seed with tractography running in the whole brain to obtain a global connectivity pattern. In the ROI-to-ROI approach, tractography was implemented between each pair of ROIs for either intrahemispheric connections (such as left AMG to left ATL) or interhemispheric connections (such as left AMG to right AMG). Fibre tracking was initiated in both directions (from seed to target and vice versa) and 25,000 streamlines were drawn from each voxel in the ROI. A binarized cerebellum mask was set as an exclusion mask for all of the analyses. The resulting three-

dimensional image files containing the output connectivity distribution were standardized using the maximum voxel intensity of each image resulting in a standardized three-dimensional image with voxel values that ranged from 0 to 1. These standardized path images were then thresholded at the 0.1 level to reduce false-positive fibre tracks. Binary connectivity maps were further generated for each individual and added across individuals. For global-connectivity-pattern and cross-hemisphere projection analyses, fibre projections that existed in more than 10% of the individuals were retained and rendered for visualization (Supplementary Fig. 1, Extended Data Fig. 1).

We used dtfit in FSL to fit a diffusion tensor model at each voxel. For each individual, the FA, mean diffusivity, radial diffusivity and axial diffusivity maps were created and the mean values for each ROI–ROI connection were extracted. The number of streamlines for each path was calculated by averaging two waytotal numbers produced by tractography. The connectivity probability for an ROI–ROI connection (such as FFA–OFA) was defined as the streamline count of that connection divided by the sum of streamline counts of all connections passing either of the ROIs (for example, there were totally 15 paths connecting either FFA or OFA)²³.

Communicability measure and community detection analysis. Communicability was quantified as the weighted sum of direct and indirect SC, in which shorter paths (that is, those with fewer steps) were weighted exponentially more heavily³⁵. For each individual (and each hemisphere), we derived a communicability map from their connectivity probability matrix. This communicability map was subsequently compared with other brain connectivity maps at the individual level to reveal the anatomy–function relationship.

At the group level, we prepared an averaged communicability map for each hemisphere for community detection analysis. Modular partitions of this averaged communicability map were obtained using the Louvain community detection method (<https://python-louvain.readthedocs.io/en/latest/>). The algorithm computes the partition of the graph nodes that maximizes the modularity using Louvain heuristics. Potential shared nodes between communities were also checked using the *k*-clique percolation method¹¹⁴ in the NetworkX toolbox (<https://networkx.github.io/>).

Analyses of major white matter bundles and superficial white matter systems.

For each hemisphere, ten major white matter bundles were identified for each individual using AFQ (<https://github.com/jyeatman/AFQ>)³⁷. We focused our analysis on six major fibre tracts that were found to be critical for face processing in a recent meta-analysis²²: the ILF, IFOF, CING, UF, SLF and AF. We also analysed four additional fasciculi provided by the AFQ algorithm (that is, thalamic radiations, corticospinal tracts, anterior and posterior corpus callosum) and found no overlap between them and all ROI–ROI connections (not reported here).

We used the atlasquery tool in FSL to evaluate the relative contribution of major fasciculi and superficial white matter to the face network²². A binarized image for each ROI–ROI connection was created for each individual and then added together across all of the individuals. We also combined all 72 bilateral connections together into one binarized image for each individual and added these images together across individuals to obtain the entire connectome image. Only voxels that existed in more than 50% of the individuals were retained (that is, the skeleton image) and were projected on two white matter atlases: the JHU white-matter tractography atlas with 48 long-range tract labels⁴¹ and the LNAO superficial white matter atlas with 79 U-shaped bundles⁴². Voxelwise analyses were then implemented to calculate the probability that the skeleton image was a member of any labelled tracts within each atlas. Note that human white matter is idiosyncratic across individuals and the two atlases that we used represent only the skeleton of the most common white matter bundles in standard MNI space; as the atlases were created by different research groups and using different methods, the two atlases are not mutually exclusive and their combination does not explain all of the face connectome voxels (that is, the sum is 92%).

PPI and FC analysis on HCP task data. The statistical model used to estimate EC and taskFC was a simple general linear regression model (GLM). We used two methods to build the generalized PPI¹¹⁵ model (using a non-deconvolution method¹¹⁶) for each seed ROI. A simple partial model had 17 separate regressors: 8 psychological regressors of task events (for example, face, body, place and tool stimuli in either 2-back or 1-back mode), 1 physiological regressor of the time series of seed ROIs and 8 corresponding interaction regressors (task events \times seed ROI's time series). A more complex full model had 25 regressors, including the identical 17 regressors in the partial model in addition to 8 extra physiological regressors of the time series of non-seed ROIs. In contrast to the partial model, the full model was designed to aggressively control for neural responses in non-seed regions.

To estimate the taskFC between the seed ROI and other ROIs, we used the contrast between regressors of task events (faces > other categories). To estimate the EC, we used the contrast between interaction regressors (PPI of faces > PPI of other categories). Z-scored β -weights were extracted for each pair of ROIs, which resulted in one 9×9 matrix for each connectivity type (taskFC or EC), each model (full or partial), each hemisphere and each individual. Although the taskFC matrices were further symmetrized, no symmetrization was applied to EC matrices

due to its directional character (that is, PPI effects indicate some information on directional neural interactions)^{45,52,53}. At the group level of the EC, one-sample *t*-tests were performed across individuals at each pair of ROIs to detect any significant effectivity connectivity. Nonparametric permutation tests (10,000 times) were also implemented to revalidate all of the significant results.

Note that all of the significant findings reported in this paper were based on the partial PPI model, as null results were found in the full model. Although a PPI model would approximate EC better as more controlled ROIs are added to the model, this approach is rarely performed in practice due to multicollinearity and the relative paucity of observations compared to potential regions (that is, degrees of freedom)⁵². Here, the null results in the full model reflect that the EC of two regions identified in the partial model might be contaminated by the influence of a third region. This methodological issue requires further exploration.

DCM on HCP task data. To validate our PPI findings, we performed DCM analyses using DCM10 in SPM8 (ref. 47). As it is common practice in DCM to restrict the analysis to a small number of nodes^{54,17}, we applied DCM to only four core face areas (EVC, OFA, FFA and STS). Motivated by our testing hypotheses (that is, the left hemisphere is feedforward whereas the right hemisphere is recurrent), we defined two simple models on the basis of PPI connectivity patterns (Fig. 4a) and tested their fitness to the observed data in each hemisphere separately. The feedforward model was derived from PPI left-hemisphere connectivity patterns (that is, face stimuli only drive feedforward processing) whereas the recurrent model was adapted from PPI right hemisphere patterns (that is, face stimuli mainly drive recurrent processing). For each model, sensory inputs started from EVC and all four ROIs were intrinsically set to be bidirectionally connected and self-connected, and their time-courses (that is, first eigenvariate) were extracted individually for each individual. To examine the modulatory effects by extrinsic face stimuli, we built a DCM GLM design matrix with six regressors (face, place, tool, body, 2-back and 0-back) and tested the two models with the face condition. To determine the optimal model, fixed-effects and random-effects group analyses were implemented using BMS¹⁸. Fixed-effects BMS assumes that the optimal model is identical across the population and uses the group Bayes factor (log-evidence) to quantify the relative goodness of models. By contrast, random-effects BMS accounts for heterogeneity of model structure across individuals and yields posterior model probabilities and exceedance probabilities.

Functional connectivity analysis on HCP resting-state data. rsFC between nine face ROIs was estimated by building nine general linear regression models. Each model defined the time series of one ROI as the dependent variable and the time series of the other eight ROIs as independent variables. For each hemisphere, Fisher-transformed correlation coefficients (*Z*-scored β -weights) were extracted for each pair of 9 × 9 ROIs, symmetrized and then averaged across two separate resting-state scans.

Comparison between different brain connectivity maps. At the individual level, we performed pairwise correlations among five brain connectivity matrices by taking all of the elements of each matrix except for the diagonal ones (self-connections), applying a Fisher's *Z*-transform and then computing the Pearson correlation. Conventional one-sample *t*-tests (against 0) were used at the group level to determine the statistical significance after controlling for multiple comparisons. Nonparametric permutation tests (10,000 times) were also implemented to revalidate all of the results.

Two different scales were examined when comparing different brain connectivity graphs: (1) at the entire face network level (72 connections in each hemisphere) or (2) at the level of only three core pathways. The core pathways were defined to include 16 core connections in each hemisphere, EVC–OFA, OFA–FFA, FFA–ATL, ATL–AMG, AMG–PCC, AMG–OFC, PCC–OFC and STS–IFG, given that they had the highest connection probability in Fig. 1a (top 25%).

We conducted multilevel mediation analyses to test whether communicability mediated the relationship between SC and rsFC. Multilevel mediation analyses were implemented using the 'Mixed linear model' function in SPSS v.25 and the models included random intercepts at the individual level. To examine the mediation at the entire face network level, we first set 72 bilateral rsFC (across all individuals) as the dependent variable *Y*, 72 corresponding communicability measures as the mediator variable *M* and 72 corresponding fibre connection probability as the independent variable *X*. We next built another model for only core pathways, with rsFC of 16 bilateral core connections as the dependent variable *Y*, 16 corresponding communicability measures as the mediator variable *M* and 16 corresponding fibre connection probabilities as the independent variable *X*.

Brain-behaviour associations. Two different statistical analyses were used to examine the brain-behaviour association—simple Pearson correlation and SVR. Pearson correlation was performed using SPSS v.25.0 and SVR was implemented using Matlab Statistics and Machine Learning Toolbox.

On the brain side, there were four independent sets of metrics: (1) neural activity profiles from 18 bilateral ROIs (the magnitude of BOLD responses to face stimuli); (2) white matter characteristics from 72 bilateral ROI–ROI connections and 20 major fasciculi; (3) 72 bilateral rsFC; and (4) 144 bilateral directional EC

during the face localizer task. On the behaviour side, we had two metrics from the HCP Penn Emotion Recognition Test—task overall accuracy (ER40_CR) and median reaction time (ER40_CRT). For each SVR analysis, we built only one model to test the association between one particular set of brain metrics (as independent variables) and one behavioural measure (as the dependent variable). For the richness of white matter properties, we tested seven microstructural measures separately (that is, FA, mean diffusivity, axial diffusivity, radial diffusivity, streamline counts, connectivity probability and tract volume size). More details about the SVR procedure are provided in the caption of Fig. 6.

To further validate that the final two parsimonious models were specific to face processing but not predictive of general performance (for example, task accuracy and reaction times), we used these models to predict other HCP non-face behavioural performance, such as the working memory 2-back task accuracy and speed (that is, WM_Task_2bk_Acc and WM_Task_2bk_RT), theory of mind judgement speed (that is, Social_Task_TOM_Median_RT_TOM) and delay-discounting ability (that is, DDisc_AUC_200).

Hemisphere lateralization. We used a two-way repeated-measures ANOVA to examine hemisphere lateralization at each level of measurements. At the neural activation level, we set the ANOVA with factors of 'hemisphere' and '9 face ROIs'. At the SC (that is, connectivity probability) or rsFC level, we set the ANOVA with factors of 'hemisphere' and '36 ROI–ROI connections'. At the EC level, we set the ANOVA with factors of 'hemisphere' and '72 directional ROI–ROI connections'. If a main effect of hemisphere was found in the ANOVA analysis, pairwise *t*-tests were further implemented to determine the hemisphere that was dominant.

To prepare for the association analysis, we computed the streamline counts ratio between intrahemispheric connections and interhemispheric connections for each face area and then averaged the ratio across two hemispheres and across all of the individuals. To define the degree of lateralization of each face area, we computed the BOLD signal ratio between the right and left area during the face localizer and averaged the ratio across individuals.

Reporting Summary. Further information on research design is available in the Nature Research Reporting Summary linked to this article.

Data availability

All data used in the present study were obtained from the WU-Minn HCP Consortium S900 Release. They are publicly available at <https://www.humanconnectome.org>.

Code availability

Most analyses were conducted using common software (FSL, SPM) or an open source toolbox that can be downloaded from GitHub (Louvain community detection algorithm, NetworkX, or AFQ toolbox). Custom codes can be accessed at https://github.com/mirrorneuronwang/HCP_face_connectome and are available from the corresponding authors on request.

Received: 29 January 2019; Accepted: 9 December 2019;
Published online: 27 January 2020

References

- Duchaine, B. & Yovel, G. A revised neural framework for face processing. *Annu. Rev. Vis. Sci.* **1**, 393–416 (2015).
- Ku, S. P., Tolia, A. S., Logothetis, N. K. & Goense, J. fMRI of the face-processing network in the ventral temporal lobe of awake and anesthetized macaques. *Neuron* **70**, 352–362 (2011).
- Kravitz, D. J., Saleem, K. S., Baker, C. I., Ungerleider, L. G. & Mishkin, M. The ventral visual pathway: an expanded neural framework for the processing of object quality. *Trends Cogn. Sci.* **17**, 26–49 (2013).
- Freiwald, W., Duchaine, B. & Yovel, G. Face processing systems: from neurons to real-world social perception. *Annu. Rev. Neurosci.* **39**, 325–346 (2016).
- Haxby, J. V., Hoffman, E. A. & Gobbini, M. I. The distributed human neural system for face perception. *Trends Cogn. Sci.* **4**, 223–233 (2000).
- Gobbini, M. I. & Haxby, J. V. Neural systems for recognition of familiar faces. *Neuropsychologia* **45**, 32–41 (2007).
- Pitcher, D., Walsh, V. & Duchaine, B. The role of the occipital face area in the cortical face perception network. *Exp. Brain Res.* **209**, 481–493 (2011).
- Collins, J. A. & Olson, I. R. Beyond the FFA: the role of the ventral anterior temporal lobes in face processing. *Neuropsychologia* **61**, 65–79 (2014).
- Wang, Y. et al. A dynamic neural architecture for social knowledge retrieval. *Proc. Natl Acad. Sci. USA* **114**, E3305–E3314 (2017).
- Mende-Siedlecki, P., Said, C. P. & Todorov, A. The social evaluation of faces: a meta-analysis of functional neuroimaging studies. *Soc. Cogn. Affect. Neurosci.* **8**, 285–299 (2013).
- Landi, S. M. & Freiwald, W. A. Two areas for familiar face recognition in the primate brain. *Science* **357**, 591–595 (2017).

12. Allison, T., Puce, a & McCarthy, G. Social perception from visual cues: role of the STS region. *Trends Cogn. Sci.* **4**, 267–278 (2000).
13. Chan, A. W.-Y. & Downing, P. E. Faces and eyes in human lateral prefrontal cortex. *Front. Hum. Neurosci.* **5**, 51 (2011).
14. O' Scailidhe, S. P., Wilson, F. A. & Goldman-Rakic, P. S. Areal segregation of face-processing neurons in prefrontal cortex. *Science* **278**, 1135–1138 (1997).
15. Troiani, V., Dougherty, C. C., Michael, A. M. & Olson, I. R. Characterization of face-selective patches in orbitofrontal cortex. *Front. Hum. Neurosci.* **10**, 279 (2016).
16. Barat, E., Wirth, S. & Duhamel, J.-R. Face cells in orbitofrontal cortex represent social categories. *Proc. Natl Acad. Sci. USA* **115**, E11158–E11167 (2018).
17. Tsao, D. Y., Schweers, N., Moeller, S. & Freiwald, W. A. Patches of face-selective cortex in the macaque frontal lobe. *Nat. Neurosci.* **11**, 877–879 (2008).
18. Tsao, D. Y., Moeller, S. & Freiwald, W. A. Comparing face patch systems in macaques and humans. *Proc. Natl Acad. Sci. USA* **105**, 19514–19519 (2008).
19. O'Doherty, J. et al. Beauty in a smile: the role of medial orbitofrontal cortex in facial attractiveness. *Neuropsychologia* **41**, 147–155 (2003).
20. Haxby, J. V. & Gobbini, M. I. Distributed neural systems for face perception. in *Oxford Handbook of Face Perception* (eds Calder, A. J., Rhodes, G., Johnson, M. H. & Haxby, J. V.) 93–110 (Oxford Univ. Press, 2012).
21. Grimaldi, P., Saleem, K. S. & Tsao, D. Anatomical connections of the functionally defined 'face patches' in the macaque monkey. *Neuron* **90**, 1325–1342 (2016).
22. Wang, Y., Metoki, A., Alm, K. H. & Olson, I. R. White matter pathways and social cognition. *Neurosci. Biobehav. Rev.* **90**, 350–370 (2018).
23. Gschwind, M., Pourtois, G., Schwartz, S., Van De Ville, D. & Vuilleumier, P. White-matter connectivity between face-responsive regions in the human brain. *Cereb. Cortex* **22**, 1564–1576 (2012).
24. Pyles, J. A., Verstynen, T. D., Schneider, W. & Tarr, M. J. Explicating the face perception network with white matter connectivity. *PLoS One* **8**, e61611 (2013).
25. Fairhall, S. L. & Ishai, A. Effective connectivity within the distributed cortical network for face perception. *Cereb. Cortex* **17**, 2400–2406 (2007).
26. Davies-Thompson, J. & Andrews, T. J. Intra- and interhemispheric connectivity between face-selective regions in the human brain. *J. Neurophysiol.* **108**, 3087–3095 (2012).
27. Van Essen, D. C. et al. The WU-Minn human connectome project: an overview. *Neuroimage* **80**, 62–79 (2013).
28. Pestilli, F., Yeatman, J. D., Rokem, A., Kay, K. N. & Wandell, B. A. Evaluation and statistical inference for human connectomes. *Nat. Methods* **11**, 1058–1063 (2014).
29. Maier-Hein, K. H. et al. The challenge of mapping the human connectome based on diffusion tractography. *Nat. Commun.* **8**, 1349 (2017).
30. Thomas, C. et al. Anatomical accuracy of brain connections derived from diffusion MRI tractography is inherently limited. *Proc. Natl Acad. Sci. USA* **111**, 16574–16579 (2014).
31. Gao, Y. et al. Validation of DTI tractography-based measures of primary motor area connectivity in the squirrel monkey brain. *PLoS One* **8**, e75065 (2013).
32. Fillard, P. et al. Quantitative evaluation of 10 tractography algorithms on a realistic diffusion MR phantom. *Neuroimage* **56**, 220–234 (2011).
33. Delettre, C. et al. Comparison between diffusion MRI tractography and histological tract-tracing of cortico-cortical structural connectivity in the ferret brain. *Netw. Neurosci.* **3**, 1038–1050 (2019).
34. Avena-Koenigsberger, A., Misis, B. & Sporns, O. Communication dynamics in complex brain networks. *Nat. Rev. Neurosci.* **19**, 17–33 (2017).
35. Crofts, J. J. & Higham, D. J. A weighted communicability measure applied to complex brain networks. *J. R. Soc. Interface* **6**, 411–414 (2009).
36. Andreotti, J. et al. Validation of network communicability metrics for the analysis of brain structural networks. *PLoS One* **9**, e0115503 (2014).
37. Yeatman, J. D., Dougherty, R. F., Myall, N. J., Wandell, B. A. & Feldman, H. M. Tract profiles of white matter properties: automating fiber-tract quantification. *PLoS One* **7**, e49790 (2012).
38. Schuz, A. & Braitenberg, V. in *Cortical Areas: Unity and Diversity* (eds Shuey, A. & Miller, R.) 377–384 (Taylor & Francis, 2002).
39. Jbabdi, S., Sotiropoulos, S. N., Haber, S. N., Van Essen, D. C. & Behrens, T. E. Measuring macroscopic brain connections in vivo. *Nat. Neurosci.* **18**, 1546–1555 (2015).
40. Wandell, B. A. Clarifying human white matter. *Annu. Rev. Neurosci.* **39**, 103–128 (2016).
41. Mori, S. et al. Stereotaxic white matter atlas based on diffusion tensor imaging in an ICBM template. *Neuroimage* **40**, 570–582 (2008).
42. Guevara, M. et al. Reproducibility of superficial white matter tracts using diffusion-weighted imaging tractography. *Neuroimage* **147**, 703–725 (2017).
43. Román, C. et al. Clustering of whole-brain white matter short association bundles using HARDI data. *Front. Neuroinform.* **11**, 73 (2017).
44. Smith, S. M. et al. Correspondence of the brain's functional architecture during activation and rest. *Proc. Natl Acad. Sci. USA* **106**, 13040–13045 (2009).
45. Stephan, K. E. On the role of general system theory for functional neuroimaging. *J. Anat.* **205**, 443–470 (2004).
46. Friston, K. J. et al. Psychophysiological and modulatory interactions in neuroimaging. *Neuroimage* **6**, 218–229 (1997).
47. Friston, K. J., Harrison, L. & Penny, W. Dynamic causal modelling. *Neuroimage* **19**, 1273–1302 (2003).
48. Cole, M. W., Bassett, D. S., Power, J. D., Braver, T. S. & Petersen, S. E. Intrinsic and task-evoked network architectures of the human brain. *Neuron* **83**, 238–251 (2014).
49. Gratton, C. et al. Functional brain networks are dominated by stable group and individual factors, not cognitive or daily variation. *Neuron* **98**, 439–452 (2018).
50. Krienen, F. M., Yeo, B. T. & Buckner, R. L. Reconfigurable task-dependent functional coupling modes cluster around a core functional architecture. *Proc. R. Soc. B* **369**, 20130526 (2014).
51. Friston, K. J. Functional and effective connectivity: a review. *Brain Connect.* **1**, 13–36 (2011).
52. Smith, D. V., Gseir, M., Speer, M. E. & Delgado, M. R. Toward a cumulative science of functional integration: a meta-analysis of psychophysiological interactions. *Hum. Brain Mapp.* **37**, 2904–2917 (2016).
53. Gerchen, M. F., Bernal-Casas, D. & Kirsch, P. Analyzing task-dependent brain network changes by whole-brain psychophysiological interactions: a comparison to conventional analysis. *Hum. Brain Mapp.* **35**, 5071–5082 (2014).
54. Stephan, K. E. et al. Ten simple rules for dynamic causal modeling. *Neuroimage* **49**, 3099–3109 (2010).
55. Honey, C. J. et al. Predicting human resting-state functional connectivity from structural connectivity. *Proc. Natl Acad. Sci. USA* **106**, 2035–2040 (2009).
56. Warren, D. E. et al. Surgically disconnected temporal pole exhibits resting functional connectivity with remote brain regions. Preprint at *bioRxiv* <https://doi.org/10.1101/127571> (2017).
57. Tyszka, J. M., Kennedy, D. P., Adolphs, R. & Paul, L. K. Intact bilateral resting-state networks in the absence of the corpus callosum. *J. Neurosci.* **31**, 15154–15162 (2011).
58. Goni, J. et al. Resting-brain functional connectivity predicted by analytic measures of network communication. *Proc. Natl Acad. Sci. USA* **111**, 833–838 (2014).
59. Grayson, D. S. et al. The rhesus monkey connectome predicts disrupted functional networks resulting from pharmacogenetic inactivation of the amygdala. *Neuron* **91**, 453–466 (2016).
60. Rousselet, G. A. & Pernet, C. R. Improving standards in brain-behavior correlation analyses. *Front. Hum. Neurosci.* **6**, 119 (2012).
61. Arbabshirani, M. R., Plis, S., Sui, J. & Calhoun, V. D. Single subject prediction of brain disorders in neuroimaging: promises and pitfalls. *Neuroimage* **145**, 137–165 (2017).
62. Fang, Y. et al. Semantic representation in the white matter pathway. *PLoS Biol.* **16**, e2003993 (2018).
63. Gottfried, J. A., Doherty, J. O. & Dolan, R. J. Encoding predictive reward value in human amygdala and orbitofrontal cortex. *Science* **301**, 1104–1107 (2003).
64. Grill-Spector, K., Weiner, K. S., Kay, K. & Gomez, J. The functional neuroanatomy of human face perception. *Annu. Rev. Vis. Sci.* **3**, 167–196 (2017).
65. Rossion, B. Constraining the cortical face network by neuroimaging studies of acquired prosopagnosia. *Neuroimage* **40**, 423–426 (2008).
66. Weiner, K. S. et al. The face-processing network is resilient to focal resection of human visual cortex. *J. Neurosci.* **36**, 8425–8440 (2016).
67. Lohse, M. et al. Effective connectivity from early visual cortex to posterior occipitotemporal face areas supports face selectivity and predicts developmental prosopagnosia. *J. Neurosci.* **36**, 3821–3828 (2016).
68. Chen, C. C., Henson, R. N., Stephan, K. E., Kilner, J. M. & Friston, K. J. NeuroImage forward and backward connections in the brain: a DCM study of functional asymmetries. *Neuroimage* **45**, 453–462 (2009).
69. He, W. & Johnson, B. W. Developmental Cognitive neuroscience development of face recognition: dynamic causal modelling of MEG data. *Dev. Cogn. Neurosci.* **30**, 13–22 (2018).
70. Bassett, D. S. & Bullmore, E. T. Small-world brain networks revisited. *Neuroscientist* **23**, 499–516 (2017).
71. Betzel, R. F. & Bassett, D. S. Specificity and robustness of long-distance connections in weighted, interareal connectomes. *Proc. Natl Acad. Sci. USA* **115**, E4880–E4889 (2018).
72. Bullmore, E. & Sporns, O. Complex brain networks: graph theoretical analysis of structural and functional systems. *Nat. Rev. Neurosci.* **10**, 312–312 (2009).
73. Wang, Y., Olson, I. R., Wang, Y. & Olson, I. R. The original social network: white matter and social cognition. *Trends Cogn. Sci.* **22**, 504–516 (2018).

74. Willems, R. M., Der Haegen, L. Van, Fisher, S. E. & Francks, C. On the other hand: including left-handers in cognitive neuroscience and neurogenetics. *Nat. Rev. Neurosci.* **15**, 193–201 (2014).
75. Levine, S. C., Banich, M. T. & Koch-Weser, M. P. Face recognition: a general or specific right hemisphere capacity? *Brain Cogn.* **8**, 303–325 (1988).
76. Bukowski, H., Dricot, L., Hanseeuw, B. & Rossion, B. Cerebral lateralization of face-sensitive areas in left-handers: only the FFA does not get it right. *Cortex* **49**, 2583–2589 (2013).
77. Eimer, M. The face-Sensitive N170 component of the event-related brain potential. in *Oxford Handbook of Face Perception* (eds Calder, A. J., Rhodes, G., Johnson, M. H. & Haxby, J. V.) 329–344 (Oxford Univ. Press, 2012).
78. Rangarajan, V. et al. Electrical stimulation of the left and right human fusiform gyrus causes different effects in conscious face perception. *J. Neurosci.* **34**, 12828–12836 (2014).
79. Ringo, J. L., Don, R. W., Demeter, S. & Simard, P. Y. Time is of the essence: a conjecture that hemispheric specialization arises from interhemispheric conduction delay. *Cereb. Cortex* **4**, 331–343 (1994).
80. Karolis, V., Corbetta, M. & Thiebaut de Schotten, M. Architecture of functional lateralisation and its relationship to callosal connectivity in the human brain. *Nat. Commun.* **10**, 1417 (2019).
81. Uddin, L. Q. et al. Residual functional connectivity in the split-brain revealed with resting-state functional MRI. *Neuroreport* **19**, 703–709 (2008).
82. Shen, K., Hutchison, R. M., Bezgin, G., Everling, S. & McIntosh, A. R. Network structure shapes spontaneous functional connectivity dynamics. *J. Neurosci.* **35**, 5579–5588 (2015).
83. Chamberland, M. et al. On the origin of individual functional connectivity variability: the role of white matter architecture. *Brain Connect.* **7**, 491–503 (2017).
84. Tsang, A. et al. White matter structural connectivity is not correlated to cortical resting-state functional connectivity over the healthy adult lifespan. *Front. Aging Neurosci.* **9**, 144 (2017).
85. Liang, H. & Wang, H. Structure-function network mapping and its assessment via persistent homology. *PLoS Comput. Biol.* **13**, e1005325 (2017).
86. Medaglia, J. D. et al. Functional alignment with anatomical networks is associated with cognitive flexibility. *Nat. Hum. Behav.* **2**, 156–164 (2018).
87. Becker, C. O. et al. Spectral mapping of brain functional connectivity from diffusion imaging. *Sci. Rep.* **8**, 1411 (2018).
88. Philippi, C. L., Mehta, S., Grabowski, T., Adolphs, R. & Rudrauf, D. Damage to association fiber tracts impairs recognition of the facial expression of emotion. *J. Neurosci.* **29**, 15089–15099 (2009).
89. Westfall, J. & Yarkoni, T. Statistically controlling for confounding constructs is harder than you think. *PLoS One* **11**, e0152719 (2016).
90. Genon, S., Reid, A., Langner, R., Amunts, K. & Eickhoff, S. B. How to characterize the function of a brain region. *Trends Cogn. Sci.* **22**, 350–364 (2018).
91. Morcom, A. M. & Fletcher, P. C. Does the brain have a baseline? Why we should be resisting a rest. *Neuroimage* **37**, 1073–1082 (2007).
92. Buckner, R. L., Krienen, F. M. & Yeo, B. T. T. Opportunities and limitations of intrinsic functional connectivity MRI. *Nat. Neurosci.* **16**, 832–837 (2013).
93. Turchi, J. et al. The basal forebrain regulates global resting-state fMRI fluctuations. *Neuron* **97**, 940–952 (2018).
94. Reveley, C. et al. Superficial white matter fiber systems impede detection of long-range cortical connections in diffusion MR tractography. *Proc. Natl Acad. Sci. USA* **112**, E2820–E2828 (2015).
95. King, D. R., de Chastelaine, M., Elward, R. L., Wang, T. H. & Rugg, M. D. Recollection-related increases in functional connectivity predict individual differences in memory accuracy. *J. Neurosci.* **35**, 1763–1772 (2015).
96. Cole, M. W. Task activations produce spurious but systematic inflation of task functional connectivity estimates. *Neuroimage* **189**, 1–18 (2019).
97. Anzellotti, S., Kliemann, D., Jacoby, N. & Saxe, R. Directed network discovery with dynamic network modelling. *Neuropsychologia* **99**, 1–11 (2017).
98. Gates, K. M. & Molenaar, P. C. M. Group search algorithm recovers effective connectivity maps for individuals in homogeneous and heterogeneous samples. *Neuroimage* **63**, 310–319 (2012).
99. Gates, K. M., Molenaar, P. C. M., Hillary, F. G. & Slobounov, S. Extended unified SEM approach for modeling event-related fMRI data. *Neuroimage* **54**, 1151–1158 (2011).
100. Smith, S. M. et al. Network modelling methods for FMRI. *Neuroimage* **54**, 875–891 (2011).
101. Gur, R. C. et al. A cognitive neuroscience-based computerized battery for efficient measurement of individual differences: standardization and initial construct validation. *J. Neurosci. Methods* **187**, 254–262 (2010).
102. McKay, N. S., Iwabuchi, S. J., Häberling, I. S., Corballis, M. C. & Kirk, I. J. Atypical white matter microstructure in left-handed individuals. *Laterality* **22**, 257–267 (2017).
103. Van Essen, D. C. et al. The human connectome project: a data acquisition perspective. *Neuroimage* **62**, 2222–2231 (2012).
104. Smith, S. M. et al. Functional connectomics from resting-state fMRI. *Trends Cogn. Sci.* **17**, 666–682 (2013).
105. Barch, D. M. et al. Function in the human connectome: task-fMRI and individual differences in behavior. *Neuroimage* **80**, 169–189 (2013).
106. Glasser, M. F. et al. The minimal preprocessing pipelines for the human connectome project. *Neuroimage* **80**, 105–124 (2013).
107. Behrens, T. E. J., Berg, H. J., Jbabdi, S., Rushworth, M. F. S. & Woolrich, M. W. Probabilistic diffusion tractography with multiple fibre orientations: what can we gain? *Neuroimage* **34**, 144–155 (2007).
108. Griffanti, L. et al. ICA-based artefact removal and accelerated fMRI acquisition for improved resting state network imaging. *Neuroimage* **95**, 232–247 (2014).
109. Weiner, K. S. et al. The mid-fusiform sulcus: a landmark identifying both cytoarchitectonic and functional divisions of human ventral temporal cortex. *Neuroimage* **84**, 453–465 (2014).
110. Coalsoun, T. S., Van Essen, D. C. & Glasser, M. F. The impact of traditional neuroimaging methods on the spatial localization of cortical areas. *Proc. Natl Acad. Sci. USA* **115**, E6356–E6365 (2018).
111. Robinson, E. C. et al. MSM: a new flexible framework for multimodal surface matching. *Neuroimage* **100**, 414–426 (2014).
112. Fox, C. J., Iaria, G. & Barton, J. J. S. Defining the face processing network: optimization of the functional localizer in fMRI. *Hum. Brain Mapp.* **30**, 1637–1651 (2009).
113. Stigliani, X. A., Weiner, X. K. S. & Grill-Spector, X. K. Temporal processing capacity in high-level visual cortex is domain specific. *J. Neurosci.* **35**, 12412–12424 (2015).
114. Palla, G., Derényi, I., Farkas, I. & Vicsek, T. Uncovering the overlapping community structure of complex networks in nature and society. *Nature* **435**, 814–818 (2005).
115. McLaren, D. G., Ries, M. L., Xu, G. & Johnson, S. C. A generalized form of context-dependent psychophysiological interactions (gPPI): a comparison to standard approaches. *Neuroimage* **61**, 1277–1286 (2012).
116. Di, X. & Biswal, B. B. Psychophysiological interactions in a visual checkerboard task: reproducibility, reliability, and the effects of deconvolution. *Front. Neurosci.* **11**, 573 (2017).
117. Hillebrandt, H., Friston, K. J. & Blakemore, S.-J. Effective connectivity during animacy perception—dynamic causal modelling of human connectome project data. *Sci. Rep.* **4**, 6240 (2015).
118. Stephan, K. E., Penny, W. D., Daunizeau, J., Moran, R. J. & Friston, K. J. Bayesian model selection for group studies. *Neuroimage* **46**, 1004–1017 (2009).

Acknowledgements

We thank K. Zhang, N. Asadi, S. Zhang, H. Zhang and R. H. Hyon for their advisory help in data analysis; A. Kohlmeyer for assistance with high-performance cluster computing; 30 undergraduates from Temple University for their work in generating and inspecting all coordinates of face ROIs, especially R. Ho, I. Hanik, P. Coleman and L. J. Hoffman. The superficial white matter atlas (LNAO-SWM79) was provided by P. Guevara. This work was supported by a National Institute of Health grant to I.R.O. (RO1 MH091113). The content is solely the responsibility of the authors and does not necessarily represent the official views of the National Institutes of Health. The work also used Temple University High Performance Cluster Service (Owlsnest), which was supported by a National Science Foundation grant (no. 1625061). The funders had no role in study design, data collection and analysis, decision to publish or preparation of the manuscript. HCP data were provided by the HCP, WU-Minn Consortium (principal investigators: D. Van Essen and K. Ugurbil; 1U54MH091657) funded by the 16 NIH Institutes and Centers that support the NIH Blueprint for Neuroscience Research; and by the McDonnell Center for Systems Neuroscience at Washington University.

Author contributions

Y.W. conceived and designed this research. Y.W., A.M., D.V.S., J.D.M., Y.Z., S.B., H.P. and Y.L. performed research and analysed data. Y.W., A.M. and I.R.O. wrote the paper. I.R.O. was principal investigator of the laboratory.

Competing interests

The authors declare no competing interests.

Additional information

Extended data is available for this paper at <https://doi.org/10.1038/s41562-019-0811-3>.

Supplementary information is available for this paper at <https://doi.org/10.1038/s41562-019-0811-3>.

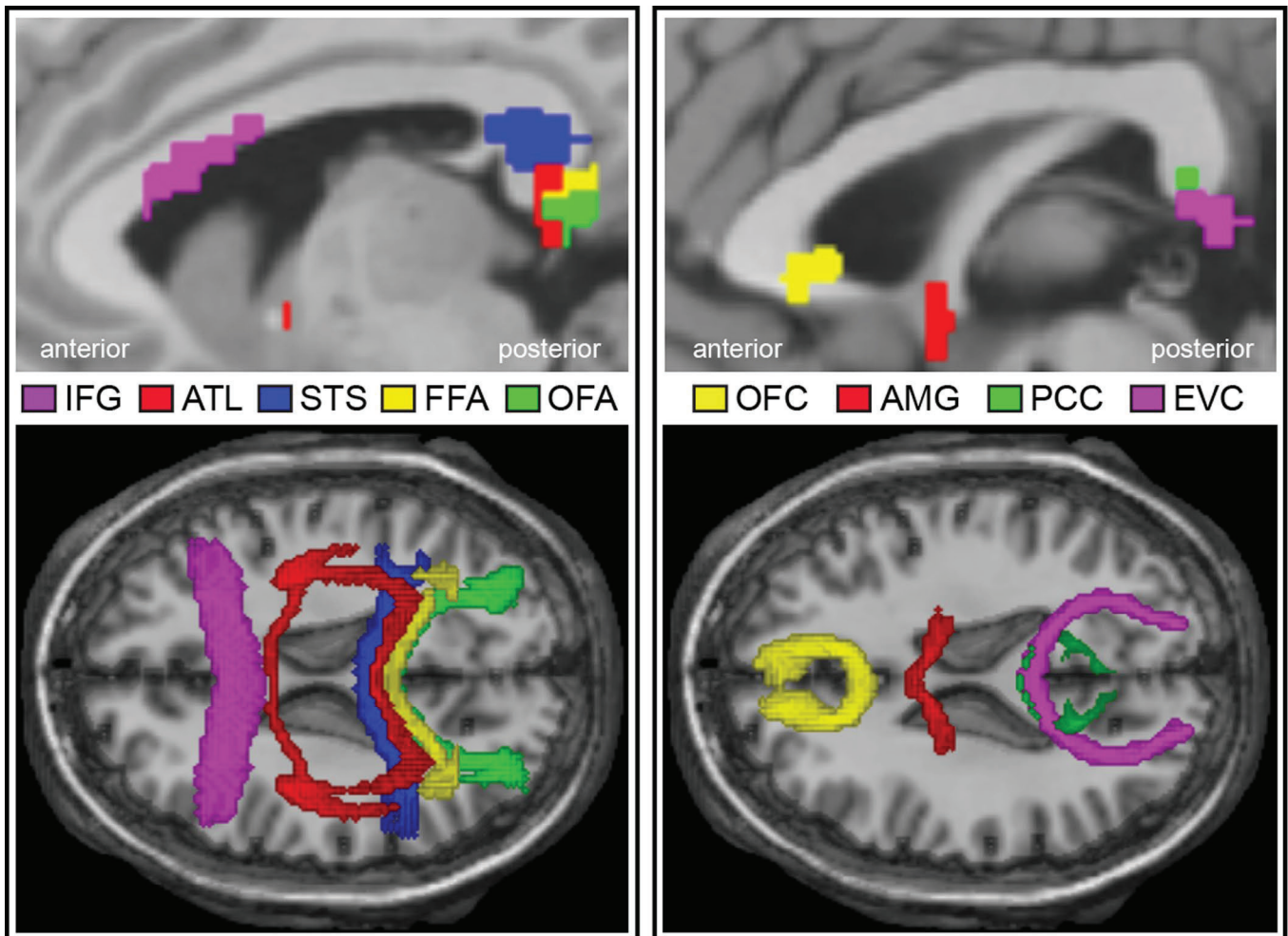
Correspondence and requests for materials should be addressed to Y.W. or I.R.O.

Peer review information Primary Handling Editor: Marike Schiffer.

Reprints and permissions information is available at www.nature.com/reprints.

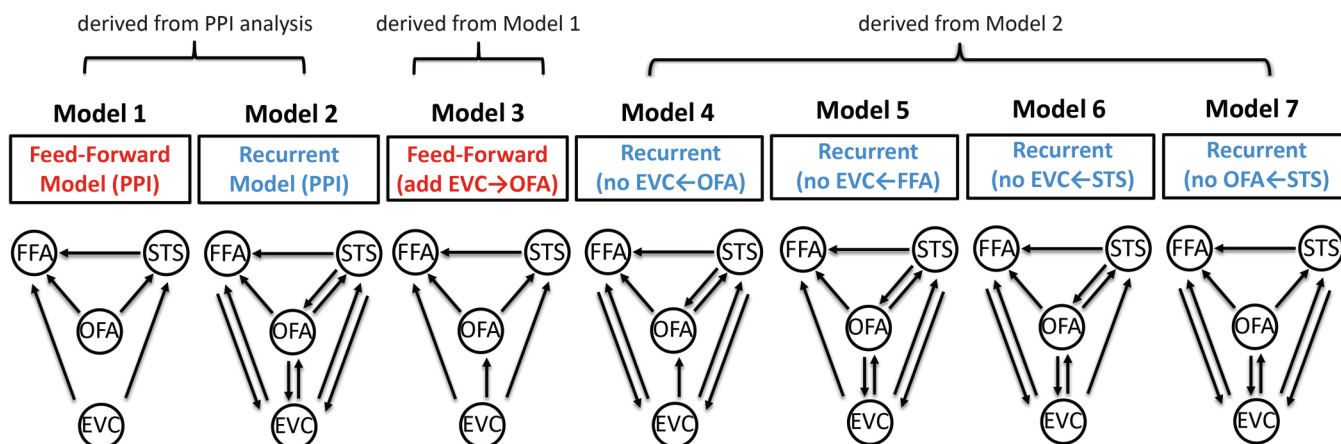
Publisher's note Springer Nature remains neutral with regard to jurisdictional claims in published maps and institutional affiliations.

© The Author(s), under exclusive licence to Springer Nature Limited 2020

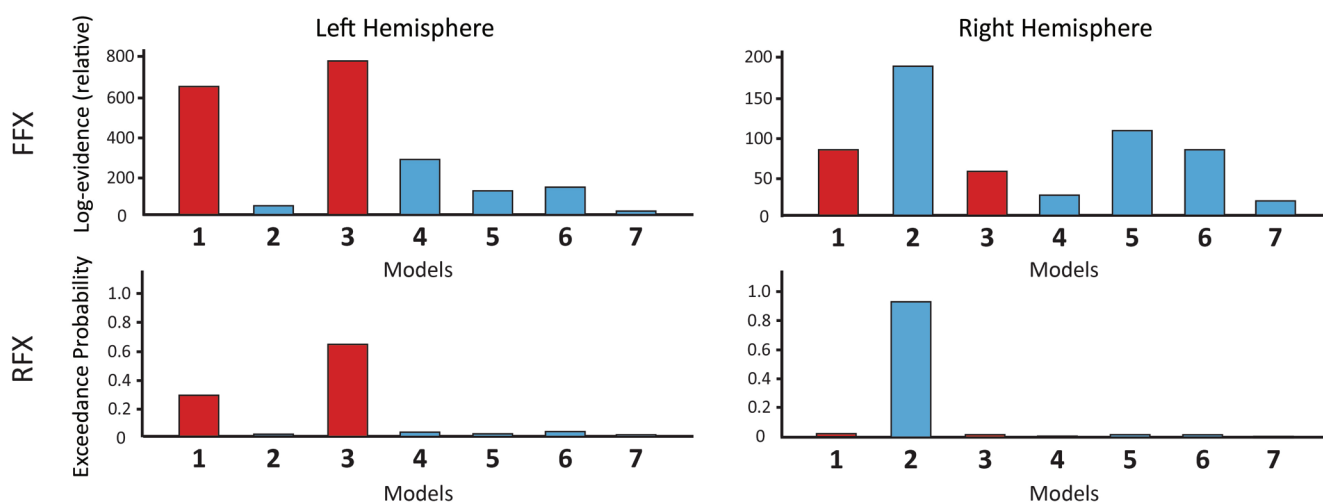


Extended Data Fig. 1 | The Interhemispheric Fibers Connecting Bilateral Face ROIs. Probabilistic tractography indicated that bilateral posterior ROIs (EVC, OFA, FFA, STS and PCC) are connected through the splenium of the corpus callosum whereas bilateral frontal ROIs are connected through the genu (IFG) or rostrum (OFC) of the corpus callosum. Bilateral ATLs have two separate interhemispheric connections, either via the splenium of the corpus callosum (by climbing up posteriorly along the temporal lobe) or the anterior commissure. Each amygdala is connected to the other by the anterior commissure. These findings accord well with previous work on the callosal fiber organization 118, AMG/ATL interhemispheric connections 119, and EVC interhemispheric connections which begin at the boundary of V1 and V2 120–122. Upper row: medial views; Lower row: axial views. Abbreviations: EVC: early visual cortex; OFA: occipital face area; FFA: fusiform face area; ATL: anterior temporal lobe; STS: superior temporal sulcus; IFG: inferior frontal gyrus; AMG: amygdala; OFC: orbitofrontal cortex; PCC: posterior cingulate cortex.

(A) DCM Model Space



(B) Bayesian Model Selection



Extended Data Fig. 2 | Additional DCM Analysis With Larger Model Space. For simplicity, we only compared two DCM models in Fig. 4. These two models, however, have limitations, given that they were merely built from preceding PPI results. For instance, the EVC→OFA connectivity is theoretically important but was not significant in the left hemisphere (LH) of PPI results (that’s why we did not include it in the original feedforward model). In addition, one might also be interested in exploring the relative contribution of each recurrent connection to the right hemisphere (RH) face processing. To address these questions, we built larger model space with seven competing models (feedforward models in red colour and recurrent ones in blue colour). (a) The first two models were the ones we used in Fig. 4. Model 1 was feedforward (based on of PPI results in LH) and Model 2 was recurrent (based on of PPI results in RH). Since Model 1 had no direct feedforward connectivity from EVC to OFA, we next built Model 3 with additional EVC→OFA. Model 4 to 7 were recurrent models modified from Model 2. As there were four recurrent connections in Model 2, we removed one feedback connection each time to examine their respective importance to the recurrent model (that is how much the model performance would suffer in the absence of a particular recurrent connection). Model 4 removed EVC←OFA; Model 5 removed EVC←FFA; Model 6 removed EVC←STS; and Model 7 removed OFA←STS. (b) Bayesian model selection (both FFX and RFX) indicates the EVC→OFA connection is important for the feedforward model, as Model 3 performs better than Model 1 in LH. This is consistent with the Haxby model suggesting the critical role of the OFA receiving information from EVC to initiate the face processing. In addition, both feedforward models perform better than any recurrent models in LH, whereas the PPI-derived recurrent model (Model 2) performed the best in RH. These results accord well with our results in Fig. 4. Moreover, among all four recurrent connections, two feedback connections (EVC←OFA, OFA←STS) seem to be particularly important for RH recurrent processing, since removal of either one can lead to enormous drop of model performance (that is Model 4 and 7). In sum, this additional DCM analysis supports our claims in Fig. 4: the LH is dominant with feedforward face processing whereas the RH is dominant with recurrent processing.